

MIXING IN EJECTA OF SUPERNOVAE. I. GENERAL PROPERTIES OF TWO-DIMENSIONAL RAYLEIGH-TAYLOR INSTABILITIES AND MIXING WIDTH IN EJECTA OF SUPERNOVAE

IZUMI HACHISU AND TAKUYA MATSUDA

Department of Aeronautical Engineering, Kyoto University, Kyoto 606, Japan

AND

KEN'ICHI NOMOTO AND TOSHIKAZU SHIGEYAMA

Department of Astronomy, University of Tokyo, Bunkyo-ku, Tokyo 113, Japan

Received 1991 March 15; accepted 1991 November 1

ABSTRACT

Nonlinear growth of two-dimensional Rayleigh-Taylor (R-T) instabilities are numerically studied to apply to the mixing in the supernova ejecta. We first present much refined calculations of mixing in the realistic model of SN 1987A with a better code and various mesh resolutions. The results show that the mixing width (or the extent of mixing) due to Rayleigh-Taylor instabilities is still too small to account for the observations even with relatively large initial perturbation. The mixing width is found to depend only slightly on the mesh resolution when the initial amplitude is larger than $\sim 5\%$ of the expansion speed.

To clarify the basic properties of the R-T instabilities and the dependence of the mixing width on the initial density structure, initial perturbation, and numerical resolution, we consider much simplified ideal models of R-T instabilities of compressible gas with an adiabatic constant $\gamma = 4/3$. The ideal R-T instabilities are calculated for various mesh resolutions, the numerical accuracy (second-order and third-order), the density ratio, the initial amplitude of the perturbations, and the mode of the initial perturbation (random from mesh to mesh and sinusoidal waves). It is found that when the initial amplitude of the velocity perturbation is larger than 1% of the sound speed, the mixing width in time depends hardly on the mesh resolution, numerical accuracy, or the mode of the initial perturbation. The mixing width depends mainly on the initial amplitudes and the density ratio. This suggests that the mixing width in the supernova ejecta depends mainly on the initial amplitude of the perturbation and on the density structure of the presupernova models (density ratio), which confirm the results on the real mixing in ejecta of SN 1987A.

Subject headings: hydrodynamics — instabilities — stars: interiors — supernovae: general — supernovae: individual (SN 1987A)

1. INTRODUCTION

Observations of SN 1987A have strongly suggested the occurrence of a large-scale mixing in the ejecta during explosion (see, e.g., Kumagai et al. 1989, and references therein). A large-scale mixing in the ejecta is also suggested for other types of supernovae (Types II-P and Ib/Ic supernovae) from the light curve modeling (e.g., Shigeyama et al. 1990) and spectrum analysis (e.g., Filippenko & Sargent 1989). In these systems, the most promising mechanism to mix the ejecta is the Rayleigh-Taylor (R-T) instability. The nonlinear growth of the R-T instability has been numerically followed by several groups and a pronounced growth of mushroom-like (or cactus-like) fingers has been confirmed in the models of SN 1987A (Arnett, Fryxell, & Müller 1989; Hachisu et al. 1990; Den, Yoshida, & Yamada 1990; Fryxell, Müller, & Arnett 1991; Müller, Fryxell, & Arnett 1992; Yamada, Nakamura, & Oohara 1990; Herant & Benz 1991, 1992). Similar calculations for Type Ib/Ic supernovae have been performed by Hachisu et al. (1991) and large-scale mixing has also been confirmed in the helium star models of Type Ib/Ic supernovae.

For SN 1987A detailed comparison between the numerical calculations and the observations has been made. Although numerical results can account for basic features of the observed properties of mixing, the expansion velocities of $\sim 3000 \text{ km s}^{-1}$ observed from the IR line width of heavy elements (e.g., Witterborn et al. 1989) and the line width of gamma-rays (Tueller et al. 1990) have failed to be reproduced in the calculations.

The effect of ^{56}Ni decay is too small to accelerate the mixed elements to the observed velocities (Herant & Benz 1991). We have to examine how the calculated mixing width depends on the numerical resolution and whether a better zoning can resolve the discrepancy. Hereafter we use the term *mixing width* to indicate the global extent of the mushroom fingers, i.e., the length of the mushroom heads from the bottom of the mushrooms.

Another problem found in the previous studies is that the R-T instability needs relatively large initial velocity perturbations to grow large, primarily because the duration of the instability is limited to within the time in which the shock propagates and breaks out of the star surface. Our preliminary numerical results (Hachisu et al. 1990) suggested that the initial amplitude of the velocity perturbation must be larger than 5% of the expansion velocity, i.e., $\gtrsim 200 \text{ km s}^{-1}$; the expansion velocity near the H/He interface is about 4000 km s^{-1} for model 14E1 (Shigeyama & Nomoto 1990) of SN 1987A when the shock arrives at the bottom of the hydrogen-rich envelope. The maximum velocity of 200 km s^{-1} is about a half of the sound speed before the shock passage. The convective motion in the presupernova star might be the source of the velocity perturbation. However, the mean velocity of the convective motion is as small as $\sim 20 \text{ km s}^{-1}$ in the helium zone and $\sim 1 \text{ km s}^{-1}$ in the hydrogen-rich envelope (based on the mixing length theory). If we start the calculation from such small amplitudes of perturbation (smaller than 1%), the development

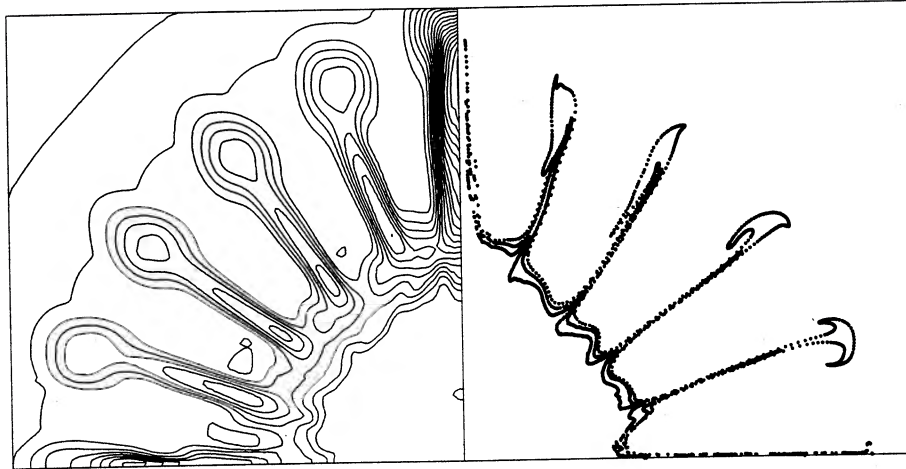


FIG. 1a

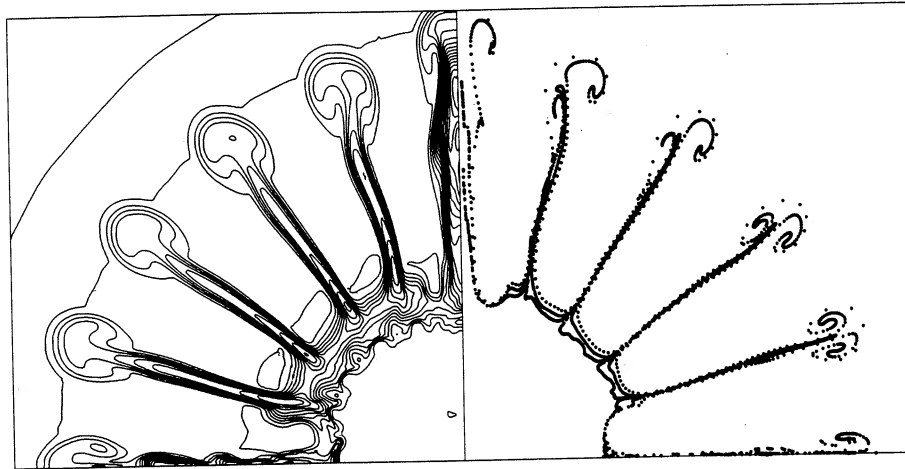


FIG. 1b

FIG. 1.—Density contours (*left*) and positions of marker particles (*right*), which are initially placed at the O/Si, He/C + O, and H/He interfaces, at $t = 14,000$ s after the explosion for an SN 1987A model (14E1). The initial perturbation is coherent (periodic). Four figures correspond to four different mesh systems, i.e., (a) 129×129 ($t = 14,002.6$ s, $R = 3.81 \times 10^{12}$ cm), (b) 257×257 ($t = 14,006$ s, $R = 3.87 \times 10^{12}$ cm), (c) 513×513 ($t = 14,001$ s, $R = 3.9 \times 10^{12}$ cm), (d) 1025×1025 ($t = 14,003$ s, $R = 3.87 \times 10^{12}$ cm).

of mixing is too small to reproduce the observations (Hachisu et al. 1990).

To examine whether these difficulties stem from the numerical problems, we first show in § 2 our new results on the mixing width in the SN 1987A model by using a third-order accurate method with several mesh resolutions. We find that the mixing width depends only slightly on the mesh resolution when the initial amplitude is relatively large, i.e., at least, larger than $\sim 5\%$ of the expansion speed as summarized in § 2 together with physical properties of the R-T mixing. Thus the difficulty to reproduce the observed large mixing width in SN 1987A remains to be resolved. These difficulties seem to be common to the previous studies in spite of significant differences in the numerical methods and initial models.

An interesting idea to resolve the above problem has been given to us by Takabe (1989) who has pointed out the possibility of an inverse cascading growth of the R-T instability: in general, shorter waves have larger growth rates in the R-T instability (e.g., Chandrasekhar 1961, chaps. X–XI; Mitchner & Landshoff 1964; Plesset & Hsieh 1964). Therefore, the very

short waves may grow to excite longer waves much faster than the linear growth rate for the corresponding longer wave through a nonlinear coupling. In usual numerical calculations, however, numerical viscosity suppresses the growth of such short waves. If the inverse cascading growth of the R-T instability operates in the ejecta of supernovae, we may resolve the difficulty mentioned above.

It is thus important to reinvestigate ideal R-T instabilities of *compressible* fluids for a wide range of parameter space. This would lead to our clearer understanding of the mixing in the supernova ejecta (the pattern and width of the R-T mixing), especially the effects of the inverse cascading growth. (Although there are several numerical calculations on the ideal R-T instability [see, e.g., the review by Sharp 1984], the parameter ranges in their studies are too narrow to apply for the present problems.) We formulate our numerical calculations of ideal R-T instabilities in § 3. The numerical accuracy of our method is examined in § 4 by comparing the numerical growth rate with the analytic one. Nonlinear growth of the R-T instability is discussed in relation to the inverse cascading growth

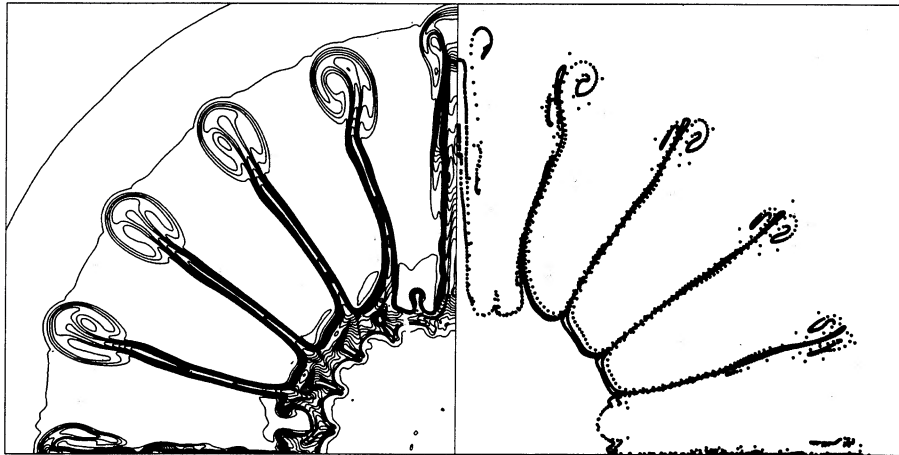


FIG. 1c

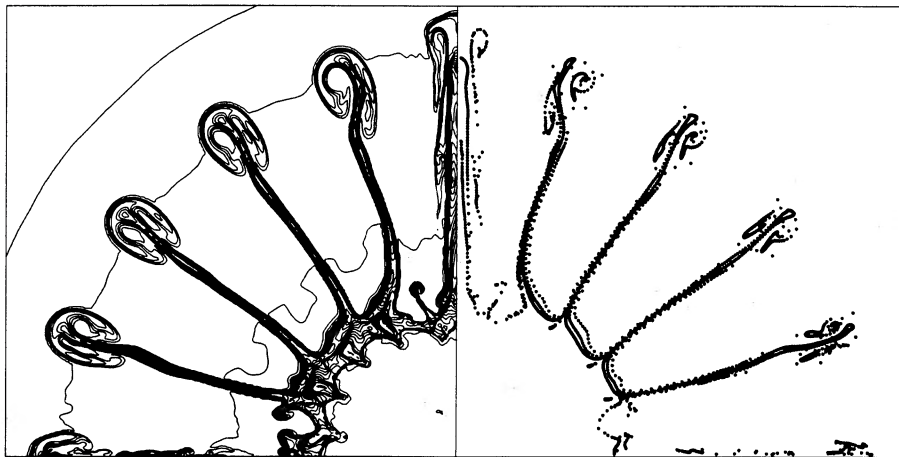


FIG. 1d

and to the mixing patterns in § 5. Width of the R-T mixing is summarized in § 6 for various conditions. Finally, our conclusions appear in § 7.

2. MIXING WIDTH IN THE MODELS OF SN 1987A

As mentioned in § 1, one important issue raised in the previous work is how the mixing width depends on the mesh resolution and the numerical accuracy. In the realistic model of SN 1987A, the density jump at the composition interface is too steep to resolve with 500–1000 mesh points in one dimension. Therefore the pattern of the mushroom fingers is rather poorly resolved if only the 500×500 mesh system is used. Here we focus more on the mixing width rather than very small-scale patterns, since the width is directly compared with the observations of SN 1987A.

Then we ask whether the mixing width is converged as the number of mesh points is increased. To answer this question, we recalculate the R-T instability in the explosion of SN 1987A by using a much better numerical code than in Hachisu et al. (1990), i.e., Roe's third-order TVD scheme (Chakravarthy & Osher 1985) which has been slightly modified to apply to strong shock waves as in supernova explosions. Assuming a constant adiabatic index $\gamma = 4/3$ to the approximate radiation dominant equation of state, axisymmetry, and equatorial sym-

metry, we start from the same initial model and perturbations (5% of the expansion velocity) as in Hachisu et al. (1990).

Nonlinear developments of the R-T instabilities at 14,000 s after the explosion of SN 1987A are seen in Figure 1 from the density contours and positions of marker particles which are initially placed at each composition interface (i.e., O/Si, He/C + O, and H/He from inside to outside). Here a coherent (periodic) perturbation of $m = 20$ is applied (see Hachisu et al. 1990). Four figures, respectively, show the results of four different mesh systems: 129×129 , 257×257 , 513×513 , and 1025×1025 . (The size of the outermost grid is 3.9×10^{12} cm.) It is clear that the mixing width is almost the same among these four cases even with 129×129 , though the mushroom patterns are more finely resolved with the finer mesh system.

To study the dependence of the mixing width on the perturbation, we calculate the case of random perturbation (R128). This initial perturbation is also the same as adopted by Hachisu et al. (1990). Figure 2 shows the density contours and positions of marker particles at $t = 14,000$ s after the explosion. Four figures also correspond to four different mesh systems, i.e., 129×129 , 257×257 , 513×513 , and 1025×1025 , respectively. Although the small-scale patterns of mushrooms are different between 257×257 , 513×513 , and 1025×1025 mesh systems, the mixing width is identical among these three cases.

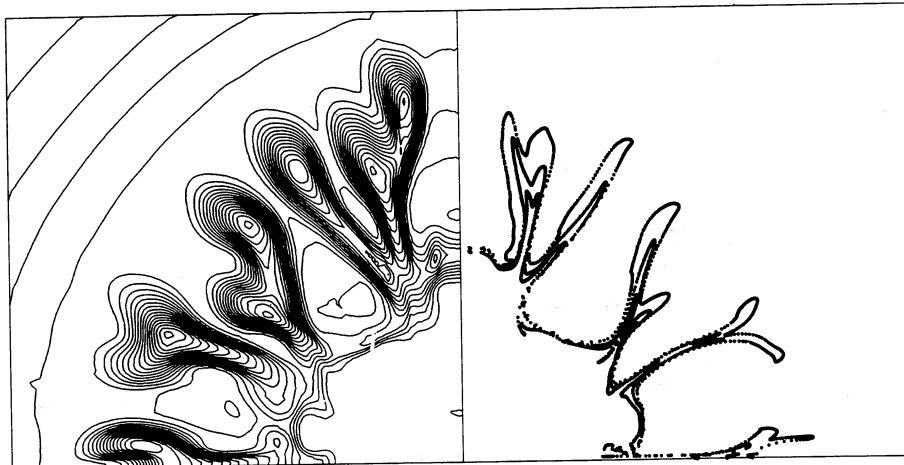


FIG. 2a



FIG. 2b

FIG. 2.—Same as Fig. 1 but for random perturbations. The time is (a) 14,000.6, (b) 14,006, (c) 14,001.9, and (d) 14,001.6 s after the explosion. The size of the box is the same as Fig. 1, i.e., $\sim 3.9 \times 10^{12}$ cm.

The conclusions from these simulations are summarized as follows:

1. For the periodic perturbation mode of $m = 20$, the width of the R-T mixing saturates once the number of mesh points in one dimension exceeds ~ 100 – 200 as far as the initial perturbation is larger than 5% of the expansion velocity.
 2. For the random perturbation mode of R128, the mixing width also saturates once the number of mesh points exceeds ~ 200 – 300 as far as the amplitude of the initial velocity perturbation is larger than 5% of the expansion velocity. The number of large-scale mushrooms also saturates at 7–8, although the number of very small-scale mushrooms is increasing with the finer mesh resolution. These conclusions are consistent with the results of previous works by Fryxell et al. (1991) and Hachisu et al. (1990).
 3. The inverse cascading growth has no large effects on the mixing width if the initial velocity perturbation is relatively large (i.e., at least larger than 5% of the expansion speed).
- With these results as well as those found for different initial models (e.g., Fryxell et al. 1991), we may tentatively argue that the mixing width observed in SN 1987A and the source of relatively large perturbation remain to be seriously studied. If so, the contributions of ^{56}Ni decay, nonsphericity in the explo-

sion, and three-dimensional effects would be essentially important.

Before reaching such conclusions, however, we need to study whether the above properties (1)–(3) are special to the models of the particular supernova SN 1987A or rather general to various cases of Rayleigh-Taylor instabilities. If the latter is found to be the case, it would explain from the general ground why the results obtained by Fryxell et al. (1991) and Hachisu et al. (1990) are essentially similar despite the differences in their numerical mesh resolutions and their initial models of explosion.

With these aims, we study the behavior of ideal Rayleigh-Taylor instabilities in the following sections. It is useful to understand basic properties of the ideal R-T mixing because the realistic models include many complicated factors and may cloud our clear understanding of the R-T mixing in the supernova ejecta.

3. COMPUTATIONAL MODELING OF RAYLEIGH-TAYLOR INSTABILITIES

Our aim is to determine the width of the R-T mixing as a function of time, which may depend on the density ratio

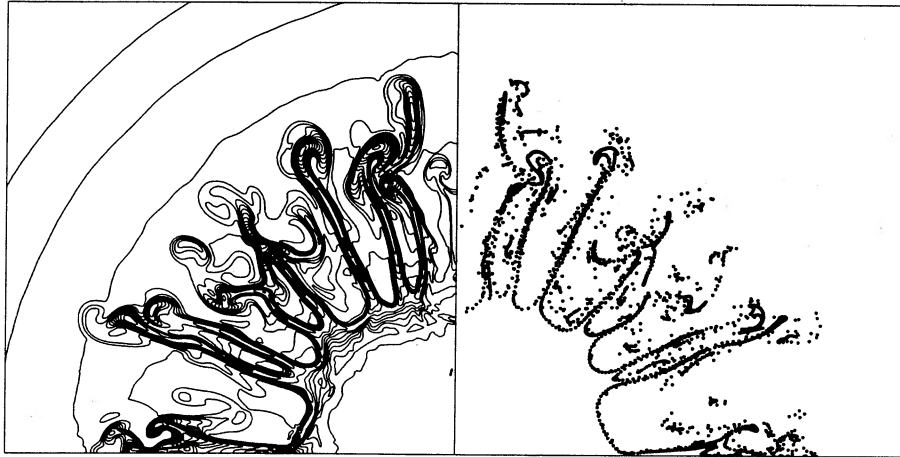


FIG. 2c

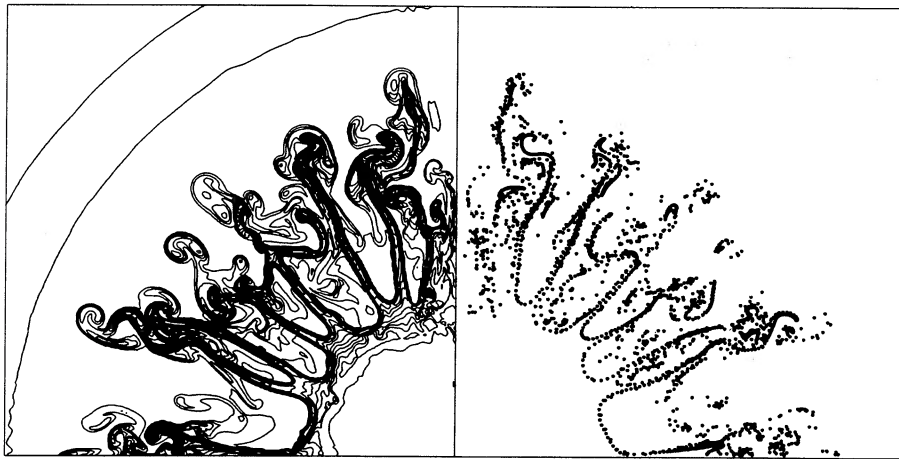


FIG. 2d

between two gases and also on the initial perturbation (amplitude and mode). The density ratio, ρ_1/ρ_2 , is closely related to the structures of presupernova models and the amplitude of the initial perturbation may be related to the convective motion just before the supernova explosion.

We set up a simplified modeling of the R-T instability for a compressible gas with an adiabatic constant $\gamma = 4/3$ (see, e.g., Chakravarthy & Osher 1985 for basic equations and numerical methods). This adiabatic assumption is a good approximation for the radiation dominant situation in the early phase of supernova explosion. Next, we assume hydrostatic equilibrium at the onset of the R-T instability, i.e., the presence of a pressure gradient. In stellar explosions, a pressure gradient is formed against the effective gravity (inertial force) when the expanding matter undergoes large deceleration. Though this effective gravity is not constant in space, we start our ideal R-T instability calculation from a hydrostatic configuration under a spatially constant gravity for simplicity.

3.1. Parameters for Initial States

We set up a square box with a length L , in which heavy gas with a constant density ρ_1 lies above light gas of ρ_2 ($\rho_1 > \rho_2$). These gases are in hydrostatic equilibrium and separated by a horizontal line at the middle of the box (see Fig. 3). The gravity is downward, and its strength g is constant for all over the box.

We normalize the physical variables with L , ρ_1 , and g , i.e., $L = 1$, $\rho_1 = 1$, and $g = 1$. Then the unperturbed state can be specified by two parameters, i.e., the pressure at the upper end of the box, P_{\min} , and the density ratio, ρ_1/ρ_2 .

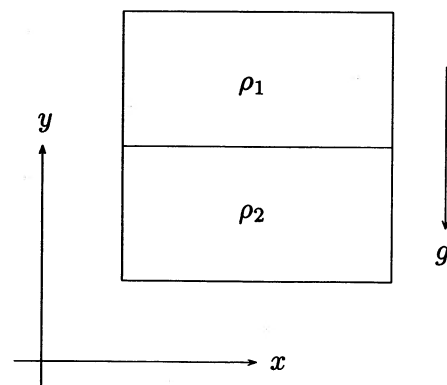


FIG. 3.—Schematic configuration of the initial state. Heavy gas lies above light gas. Each has a uniform density as indicated in the figure. The gravity g is downward and constant in space. The initial state is in hydrostatic balance.

3.2. Numerical Method and Boundary Conditions

We solve the Euler equations with a constant adiabatic index $\gamma = 4/3$ on a Cartesian coordinate system with x -axis being horizontal and y -axis being vertical (see Fig. 3). Each direction is divided with an equal mesh interval. The numerical method is a third-order Roe scheme with a TVD (total variation diminishing) flux limiter (Chakravarthy & Osher 1985). Though this numerical scheme is complicated, we have succeeded to completely vectorize the code, thus making the calculation as fast as $\sim 0.2 \times 10^6$ zones per second on a single Fujitsu VP-400E processor. Therefore, one case can be computed in 5 minutes ($x \times y = 128 \times 128$ and 3000 steps) or 40 minutes (256×256 and 6000 steps) CPU time on a VP-400E.

We assume a periodic boundary condition in the x -direction. For the y -direction, an ambient condition is used at the upper and the lower boundaries, where "ambient" means that the physical variables outside the boundary are constant in time.

3.3. Initial Perturbations

Two types of perturbations are assumed at the initial kickoff to see the dependence of the nonlinear growth of the R-T instability on the mode of perturbation: (1) periodic sinusoidal perturbation, which is represented by

$$v_{i,j} = c_{i,j} \epsilon \cos(m2\pi x_i/L), \quad (1)$$

and (2) random perturbation (which is applied to the velocity field at each mesh),

$$v_{i,j} = c_{i,j} \epsilon (2 \text{ rmd}(i) - 1), \quad (2)$$

where v is the velocity in the y -direction, $\text{rmd}(i)$: integer) is a function which produces a uniform random number between 0 and 1, ϵ is the amplitude of the perturbation, and $c_{i,j}$ the local sound speed at mesh point (i, j) .

In most cases, we perturb the velocity field for all mesh points. In some cases, the perturbation area is limited within the lower half of the box in order to simulate the cases where the initial perturbation is originated from the convection only in the H- or He-burning shell.

Our two-dimensional calculations are performed for many combinations of the density ratio ($\rho_1/\rho_2 = 1.5, 3,$ and 10), the initial amplitude ($\epsilon = 0.16, 0.04, 0.01, 10^{-3}, 10^{-4},$ and 10^{-6}), the types of mode (sinusoidal with m and random), the number of grids ($x \times y = 128 \times 128$ and 256×256), and the perturbed area (whole and a lower half). These are summarized in Tables 1–3. To examine the width of mixing, we follow the positions of 3075 marker particles which are initially placed at the interfaces between the two gases. The pressure at the upper end of the box, P_{min} , is fixed to be 0.1 for all models.

4. NUMERICAL TEST WITH LINEAR GROWTH RATES

The linear growth rate α of the R-T instability is analytically obtained for the small wavelength limit of compressible fluids with a sharp boundary as (Mitchner & Landshoff 1964),

$$\alpha = \left[\frac{(dp_0^-/dy)_0 - (dp_0^+/dy)_0}{\rho_+ + \rho_-} k \right]^{1/2}, \quad (3)$$

where k is the wave number and the suffixes $+$ and $-$ mean the physical value at the upper and lower part of the interface, respectively. In our case of Figure 3, this formula is reduced to

$$\alpha = \left(\frac{\rho_1 - \rho_2}{\rho_1 + \rho_2} gk \right)^{1/2}, \quad (4)$$

where g is the gravity. (Note that $g = 1$ in our case and $k = 2\pi/\lambda$, where λ is the wavelength.) Equation (4) is exactly the same as that for incompressible gases (Chandrasekhar 1961). The velocity of the gas motion in the linear regime is so small compared with the sound speed that the effect of compressibility is negligible. Therefore, the linear growth rate for compressible gas should be very close to that for incompressible

TABLE 1
MODEL PARAMETERS OF 128×128 GRIDS

Number of Run	Perturbed Region	ρ_1/ρ_2	Mode	ϵ
1	whole	3	S1	10^{-4}
2	whole	3	S1	10^{-3}
3	whole	3	S1	0.01
4	whole	3	S1	0.04
5	whole	3	S1	0.16
6	whole	3	S2	10^{-4}
7	whole	3	S2	10^{-3}
8	whole	3	S2	0.01
9	whole	3	S2	0.04
10	whole	3	S2	0.16
11	whole	3	S4	10^{-4}
12	whole	3	S4	10^{-3}
13	whole	3	S4	0.01
14	whole	3	S4	0.04
15	whole	3	S4	0.16
16	whole	3	S8	10^{-4}
17	whole	3	S8	10^{-3}
18	whole	3	S8	0.01
19	whole	3	S8	0.04
20	whole	3	S8	0.16
21	whole	3	S16	10^{-4}
22	whole	3	S16	10^{-3}
23	whole	3	S16	0.01
24	whole	3	S16	0.04
25	whole	3	S16	0.16
26	whole	3	S32	10^{-4}
27	whole	3	S32	10^{-3}
28	whole	3	S32	0.01
29	whole	3	S32	0.04
30	whole	3	S32	0.16
31	whole	3	R128	10^{-6}
32	whole	3	R128	10^{-4}
33	whole	3	R128	10^{-3}
34	whole	3	R128	0.01
35	whole	3	R128	0.04
36	whole	3	R128	0.16
37	whole	10	S1	0.01
38	whole	10	R128	0.01
39	whole	10	S1	0.04
40	whole	10	R128	0.04
41	whole	10	S1	0.16
42	whole	10	R128	0.16
43	whole	1.5	S1	0.01
44	whole	1.5	R128	0.01
45	whole	1.5	S1	0.04
46	whole	1.5	R128	0.04
47	whole	1.5	S1	0.16
48	whole	1.5	R128	0.16
49 ^a	whole	3	R128	10^{-6}
50 ^a	whole	3	R128	0.01
51	lower half	3	S1	10^{-3}
52	lower half	3	S1	0.01
53	lower half	3	R128	10^{-6}
54	lower half	3	R128	10^{-3}
55	lower half	3	R128	0.01

^a Second-order accuracy.

TABLE 2
MODEL PARAMETERS OF 1024 × 16 GRIDS

Number of Run	Perturbed Region	ρ_1/ρ_2	Mode	ϵ
56.....	whole	3	S1	10^{-4}
57.....	whole	3	S2	10^{-4}
58.....	whole	3	S4	10^{-4}
59.....	whole	3	S8	10^{-4}
60.....	whole	3	S16	10^{-4}
61.....	whole	3	S32	10^{-4}

gas, so that we may use equation (4) for a numerical test of our code.

To pick up the amplitude of corresponding wavenumber, k , we make a FFT (fast Fourier transformation) of the velocity on the horizontal line at the middle of the box. Figure 4 shows the amplitude, $(a_n^2 + b_n^2)^{1/2}$, of each mode for the initial perturbation of $m = 2$ in equation (1), where a_n and b_n are the coefficient for $\cos(2\pi nx/L)$ and $\sin(2\pi nx/L)$ components, respectively, and n is related to the wavenumber k by $n = k/2\pi$. The amplitude for $n = 2$ increases exponentially from $t = 0.5$ to $t = 3$.

We then numerically determine the linear growth rate of the R-T instability from these slopes. Figure 5 depicts the growth rates thus obtained for various n and mesh systems. The dashed line represents the analytic growth rate of equation (4). It is clear that relatively longer waves are finely resolved, whereas the growth rates for shorter ones are suppressed due to numerical viscosity. For the grids of $x \times y = 128 \times 128$, 256×256 , and 1024×16 , our code does finely resolve the growth rate (being very close to the dashed line in Fig. 5) up to $n = 8, 16$, and 32, respectively.

These results imply that more than 8–10 grids per one wave are necessary to finely resolve the linear growth rate in our numerical code. In other words, the growth of the R-T instability can be followed if we prepare more than 10 meshes for each mushroom structure of the R-T instabilities. This rough estimation may consistently explain the convergence of the mixing width in SN 1987A models (see § 2). Note that no prominent growth of the R-T instability is obtained in several dynamical times if we impose no initial perturbation ($\epsilon = 0$).

5. NUMERICAL RESULTS FOR NONLINEAR REGIME

The growth of the R-T instability has been followed until two gases are completely mixed in the box. Prominent proper-

TABLE 3
MODEL PARAMETERS OF 256 × 256 GRIDS

Number of Run	Perturbed Region	ρ_1/ρ_2	Mode	ϵ
62.....	whole	3	S1	10^{-4}
63.....	whole	3	S1	10^{-3}
64.....	whole	3	S1	0.01
65.....	whole	3	S2	10^{-4}
66.....	whole	3	S4	10^{-4}
67.....	whole	3	S8	10^{-4}
68.....	whole	3	S16	10^{-4}
69.....	whole	3	S32	10^{-4}
70.....	whole	3	R256	10^{-6}
71.....	whole	3	R256	10^{-3}
72.....	whole	3	R256	0.01
73.....	whole	10	R256	10^{-6}
74.....	whole	1.5	R256	10^{-6}
75.....	lower half	3	S1	10^{-3}
76.....	lower half	3	R256	10^{-3}
77.....	lower half	3	R256	0.01

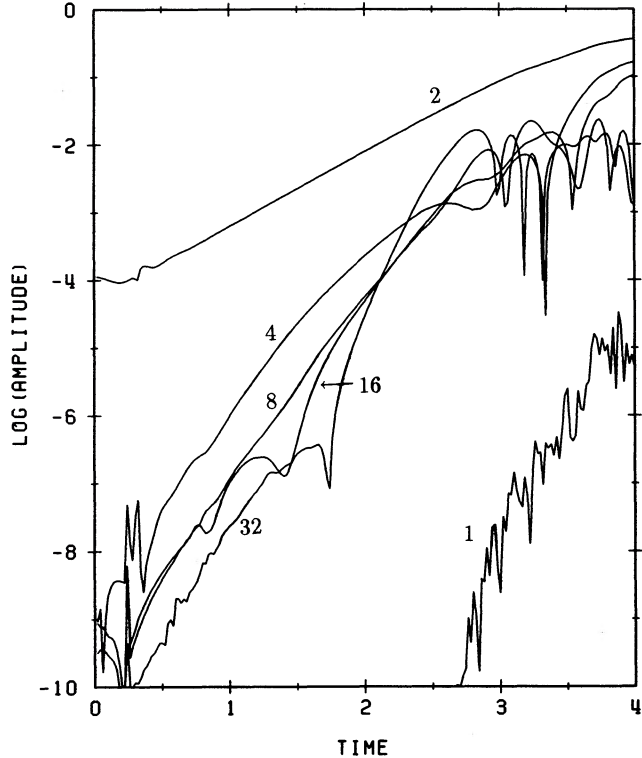


FIG. 4.—Amplitude of each sinusoidal mode is plotted as a function of the time for the case of $m = 2$ in eq. (1). Grid size is 256×256 . The numbers attached indicate $n = 1/\lambda$. The amplitude for $n = 2$ mode linearly grow from $t = 0.5$ to $t = 3$. The numerical growth rate for $n = 2$ is obtained from this slope.

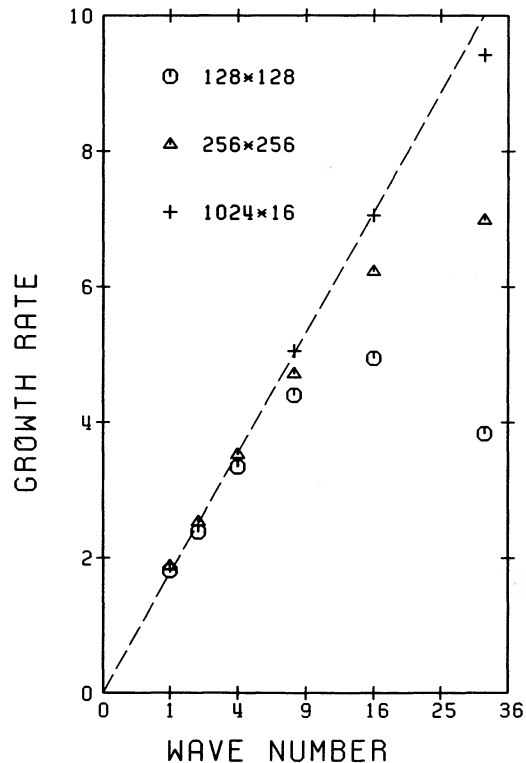


FIG. 5.—Numerical growth rates obtained for each mode are plotted against $n = k/2\pi = 1/\lambda$. The dashed line denotes the analytic growth rate of eq. (4). The numerical growth rate saturates for shorter waves due to numerical viscosity.

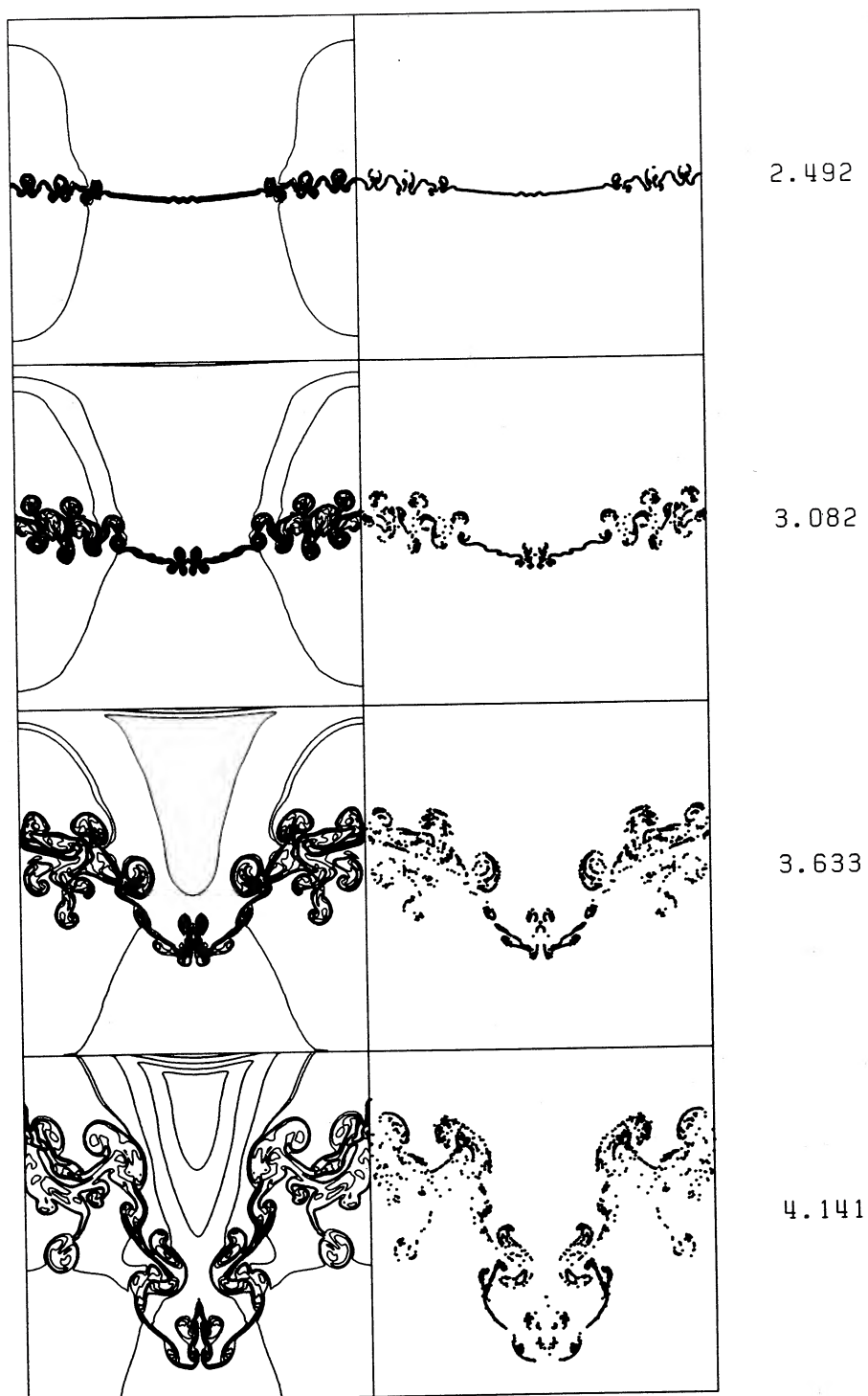


FIG. 6a

FIG. 6.—Density contour (*left*) and the positions of marker particles (*right*) are shown in time sequence. Grid size is 256×256 . Each contour is linearly spaced with 10% of the difference between the highest and the lowest densities. The time elapsed is shown in the right side of the box. (a) $m = 1$, $\epsilon = 10^{-3}$, $\rho_1/\rho_2 = 3$, (run 63 in Table 3); (b) $m = 2$, $\epsilon = 10^{-4}$, $\rho_1/\rho_2 = 3$, (run 65 in Table 3); and (c) $m = 4$, $\epsilon = 10^{-4}$, $\rho_1/\rho_2 = 3$, (run 66 in Table 3), respectively.

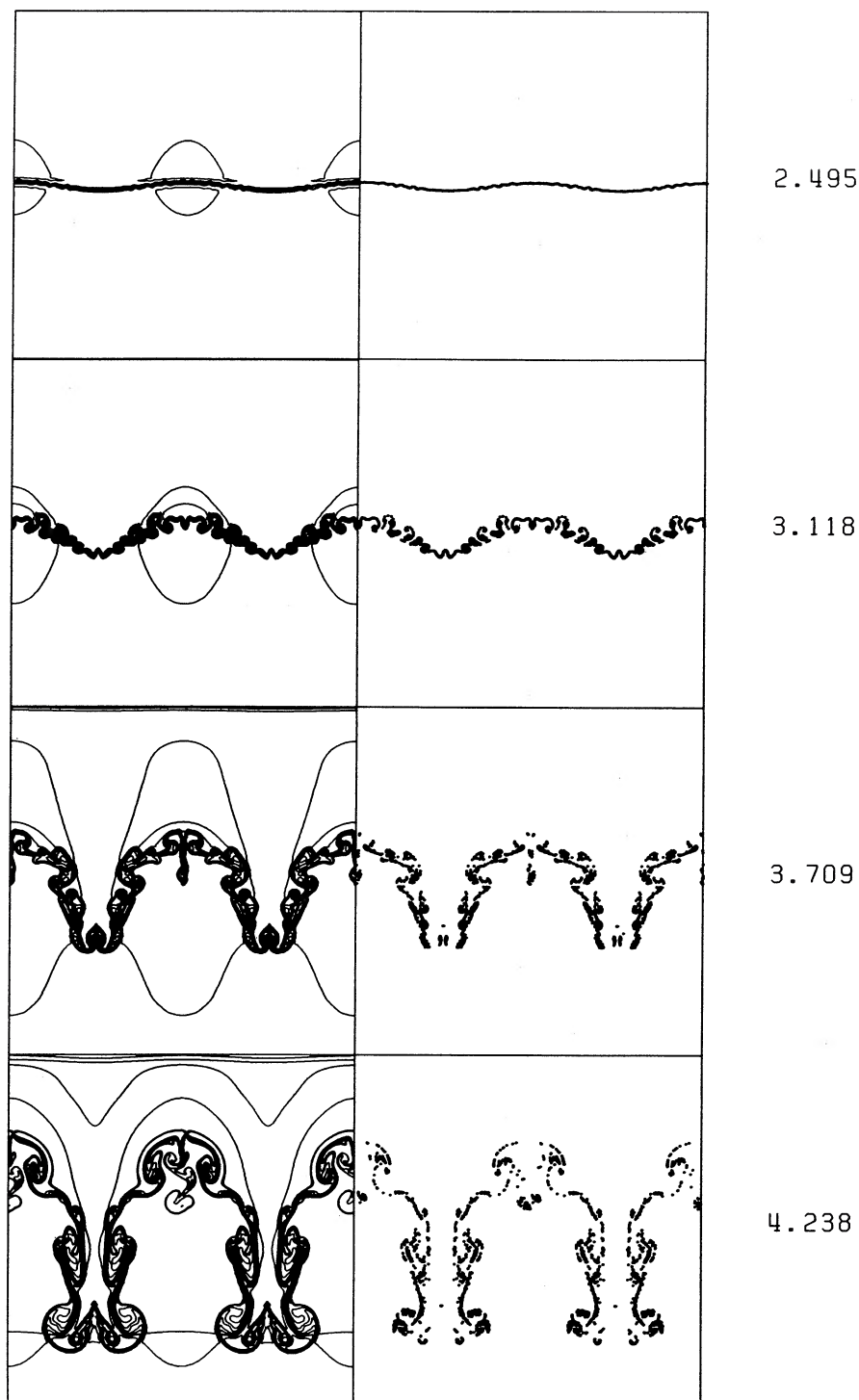


FIG. 6b

ties of the nonlinear growth of the R-T instabilities are as follows.

5.1. Fractal Fingering

First interesting feature is a fractal structure at the interface between two gases. Figure 6 shows the time development of the R-T instability on the 256×256 grids. We have started the calculation from the periodic sinusoidal modes of $m = 1$,

$m = 2$, and $m = 4$ with a relatively small initial amplitude, $\epsilon = 10^{-3}$, $\epsilon = 10^{-4}$, and $\epsilon = 10^{-4}$, respectively, as seen in Figures 6a, 6b, and 6c.

We observe that several waves with small wavelengths grow faster than the original waves of $m = 1$ and $m = 2$ at the interface in Figures 6a and 6b. The origin of these short waves is the truncation error in our numerical code so that we cannot control or suppress their growth. This nature essentially stems

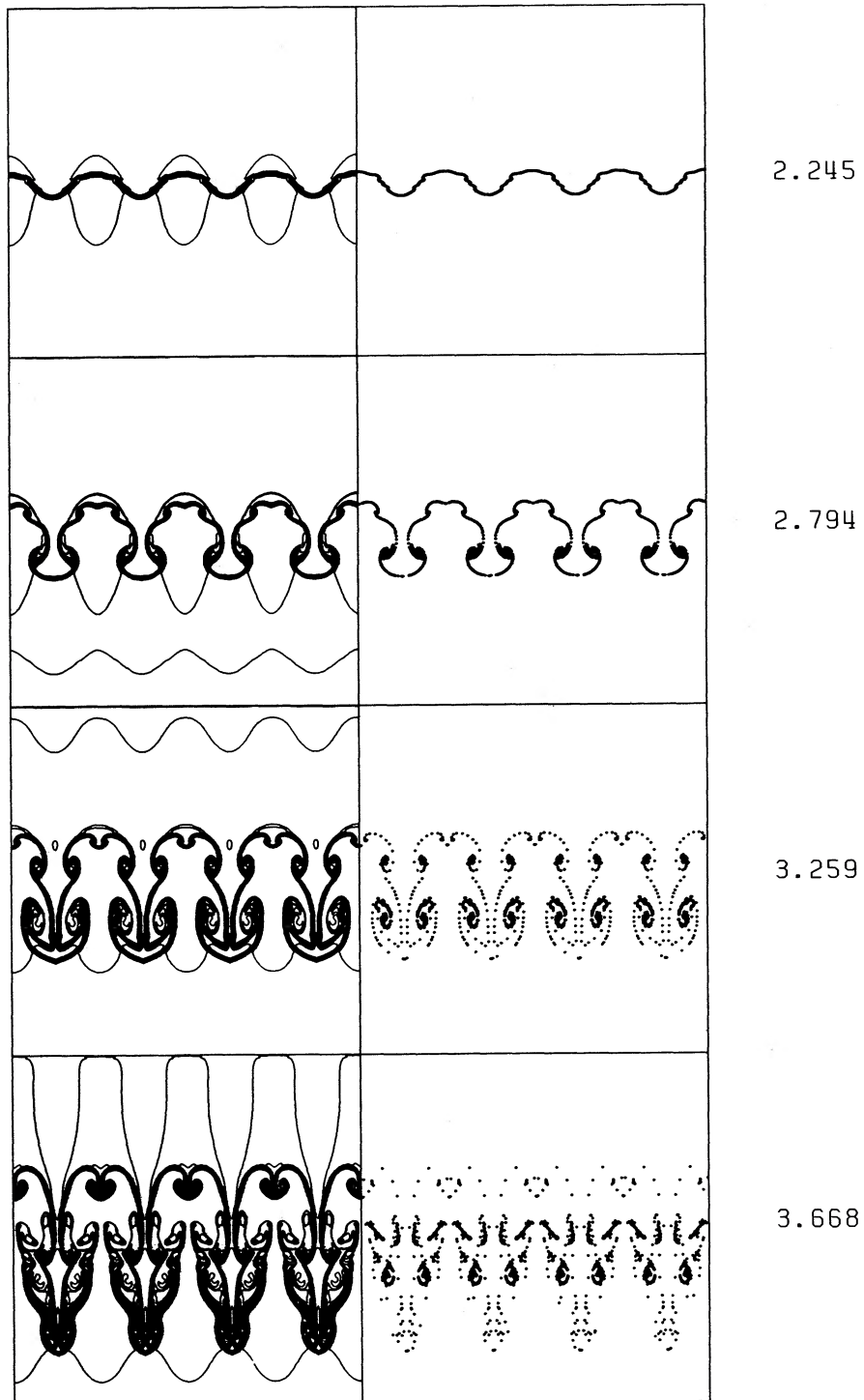


FIG. 6c

from the linear growth rate of the R-T instability, i.e., equation (4). Even though the initial amplitude of the shortest wave is very small, its growth rate is much larger than the original long waves. The shortest one eventually takes over the longer ones. If the initial amplitude is 10 times larger, i.e., $\epsilon = 0.01$ for the $m = 1$ sinusoidal mode, the growth of higher modes is not so prominent as shown in Figure 7. This is because the time is too short for higher modes to grow large before the original long

wave grows. (Compare the elapsed time after the initial kickoff between Fig. 6a and 7.) Once a large-scale mushroom structure develops, the interface between the two gases is no longer a horizontal line so that the simple growth rate of equation (4) cannot be applied; then the Kelvin-Helmholtz type instability at the interface becomes important.

To clearly show the growth of higher modes which come from the truncation errors for the model in Figure 7, we have

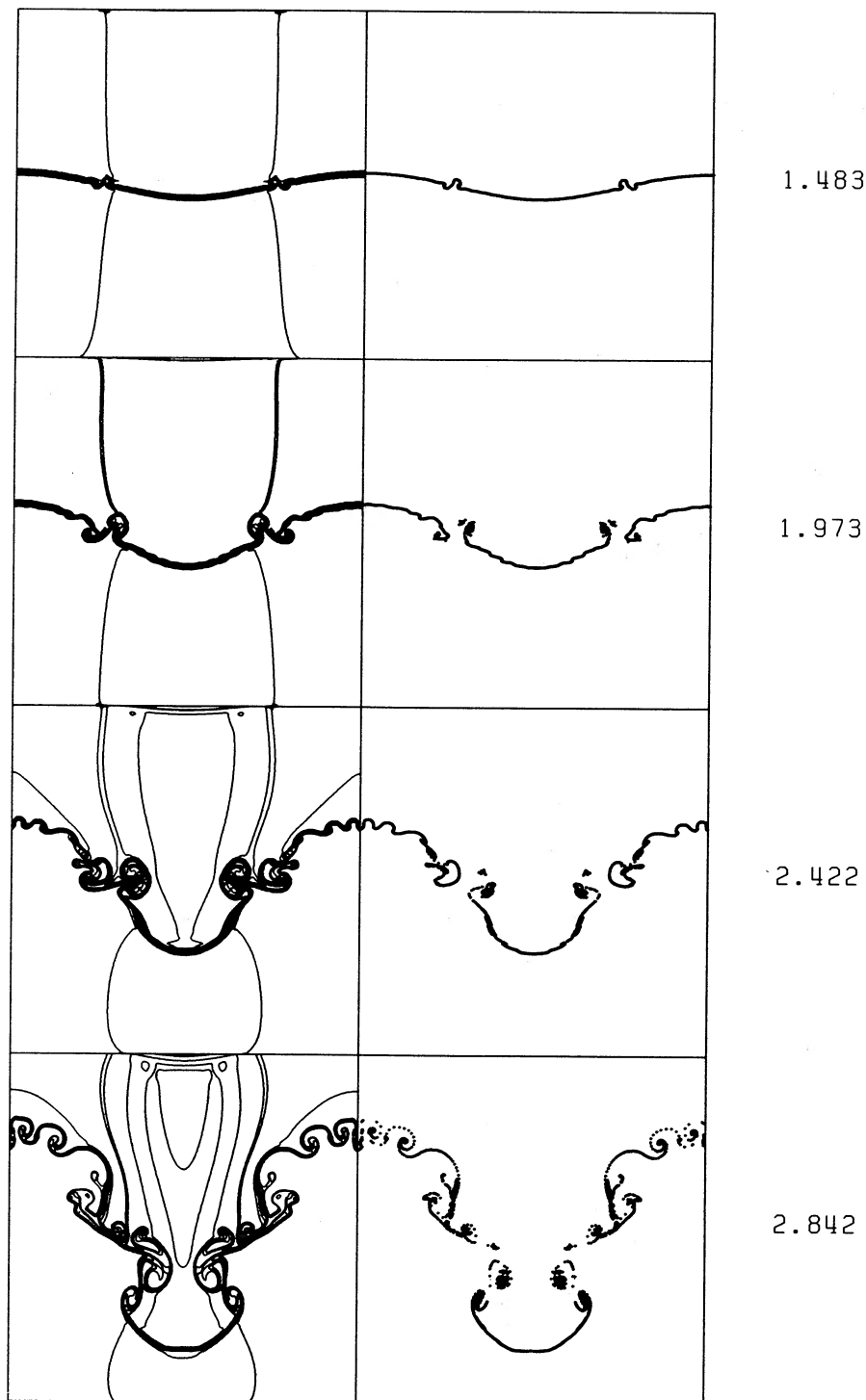


FIG. 7.—Same as Fig. 6a but for a larger initial amplitude of $\epsilon = 0.01$ (run 64 in Table 3). The fractal fingering structures are not so prominent compared with those of Fig. 6a.

plotted a time development of the spectrum, i.e., the amplitude, $(a_n^2 + b_n^2)^{1/2}$, against $n = k/2\pi$ in Figure 8.

At $t = 0$, there exists only one component, $n = 1$. All other components, $n > 1$, are excited only in one time step because of the truncation error in our numerical code. These higher modes grow at a rate of equation (4), which is much larger than

the original one (the growth rate for $n = 1$). Eventually, the highest mode catches up with the lower ones at $t \sim 1.5$. We will call these features *fractal fingering* only when much smaller scale fingers grow faster than the original longer waves. When the perturbation is random, we cannot define this *fractal fingering* because the original waves already contain the shortest

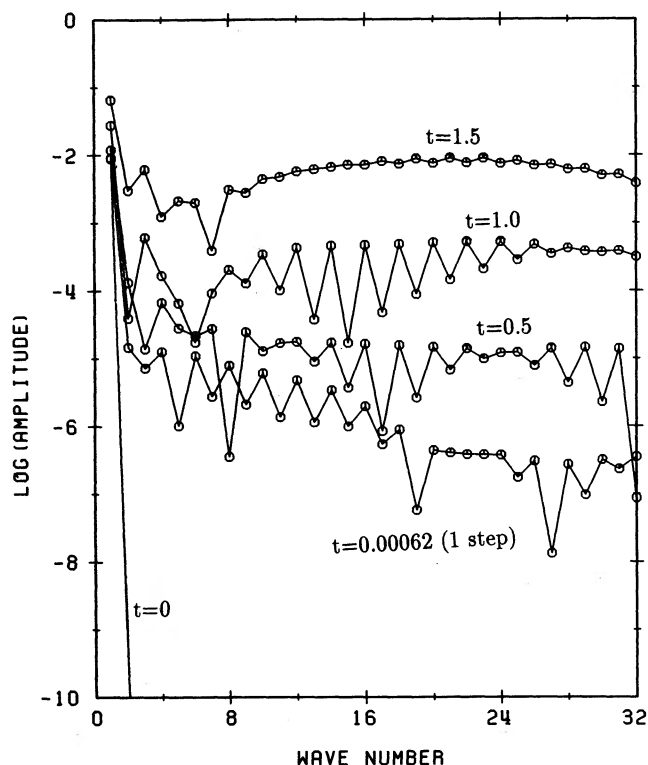


FIG. 8.—Time development of the spectrum is shown for the model of Fig. 7. The spectrum is the amplitude of the velocity field on the horizontal line at the half of the box.

wavelength with a finite amplitude at $t = 0$. In this sense, we may use the word *fractal fingering* only when the perturbation is sinusoidal or much longer than the mesh resolution.

To examine the mesh-dependence of such fractal fingering structures, we have plotted time development of the R-T instability for two models starting from the same initial perturbation but with the different grid points. Figures 9 and 10 show the fractal structures at the interface for the 128×128 and 256×256 grids, respectively. It is seen that the shortest waves in the 128×128 mesh are longer by a factor of ~ 2 than those in the 256×256 mesh, but the global structures are almost the same.

In Figures 9 and 10, the shortest waves for the 128×128 and 256×256 grids have wavelengths of $\lambda \sim \frac{1}{20}$ and $\frac{1}{40}$, respectively. These are very close to the modes having the largest linear growth rates in Figure 5. This suggests that the small-scale structures or patterns of the R-T instabilities would not be resolved even if we enormously increase the number of grids. It is also expected that the interface is smeared out by the small-scale R-T mixing. Though this kind of characteristic (fractal fingering) is sometimes mentioned and known as the *ill-posed* problem of the R-T instability without viscosity or surface tension (e.g., Sharp 1984), the present result is a clear demonstration to show the dependency of the fractal fingering on the mesh resolution.

It should be emphasized that, to observe this kind of fractal fingering, the initial amplitude of the perturbation must be as small as $\sim 0.1\%$ of the expansion velocities of the supernova ejecta. Figure 11 shows the development of *fractal fingering* in supernova (SN 1987A: model 14E1), which means that the fingers with scales much smaller than the original scale of per-

turbation grow faster. Here we impose an initial perturbation of mode M20 (i.e., $m = 20$) and 0.2% amplitude. If we start from a relatively large initial amplitude such as 5%, however, we do not observe this kind of fractal fingering but find only simple mushroom fingers as seen in Figure 1. Although there is a long history of calculations of idealized R-T instabilities in the literature, many of them were started from a periodic (sinusoidal) perturbation with a relatively large amplitude, thereby being unable to clearly show such a fractal fingering as seen in Figures 9, 10, and 11 (e.g., see Figs. 1 and 7 of Youngs 1984).

In Figures 9 and 10, the initial perturbation is introduced only in the lower half of the box. Therefore the total kickoff energy at $t = 0$ is smaller and thus the global structure grows slower in Figure 10 than in Figure 6a for the same ϵ (compare the elapsed time in the figures). This implies that when the perturbation is originated from the convective motion and limited to within the lower half region, the mixing width of the R-T instability is smaller than in the case of whole perturbation. (The fractal fingering develops more in Fig. 10 than in Fig. 6a simply because of the short elapsed time in Fig. 6a.)

5.2. Inverse Cascading Growth

In the realistic situation, random perturbation is more likely the case than the periodic sinusoidal perturbation. Figures 12a and 12b show the nonlinear growth of the R-T instability for random perturbation on the 128×128 and 256×256 grids, respectively. It is observed that the pattern of mixing is gradually changing from shorter scales to longer scales. This kind of characteristic is called *inverse cascading growth* (e.g., Read 1984; Youngs 1984; Wang & Robertson 1985).

To quantitatively show these kind of properties, we plot in Figure 13 the evolution of the spectrum for the case in Figure 12b (256×256 grids). The spectrum is white noise at $t = 0$ because of a uniform random perturbation. Considering the resolution of 256×256 grids, we plot the spectrum up to $n = 32$. It is seen that the shorter waves grow much faster than the longer ones. At $t \sim 2$, the growth of the shorter ones saturates because of nonlinear effects. After this phase, the longer waves still grow and eventually take over the shorter ones.

Figure 13 also shows that the growth rates of the shortest waves are very close to the linear growth rate predicted by equation (4), but the growth rates for the longest ones are much greater than that of equation (4). This implies that energy is transferred from the shorter waves to the longer waves as a result of nonlinear coupling. To see this, we also plot the growth of each n in Figure 14. The amplitudes of $n = 16$ and $n = 32$ are linearly growing from $t = 0.2$ to $t = 1.5$ so that the growth rates are very close to those in Figure 5 (i.e., the growth rates of $n = 16$ and 32 for the 256×256 grids). These amplitudes saturate at $t \sim 1.5$. The amplitudes of longer waves $n = 1, 2, 4,$ and 8 also grow linearly until $t = 1.2$ – 1.5 . Then the growth rates suddenly increase and catch up with the shortest modes at $t \sim 2$. The growth rates of $n = 32$ and 16 slightly decrease during this period of $t = 1.5$ – 2 . This clearly shows that energy is transferred from the shortest modes to the longer ones.

6. WIDTH OF RAYLEIGH-TAYLOR MIXING

For the supernova problems, it is important to know the width of the mixing due to the R-T instability. In this section, we focus on what is the most important factor that determine the width of mixing.

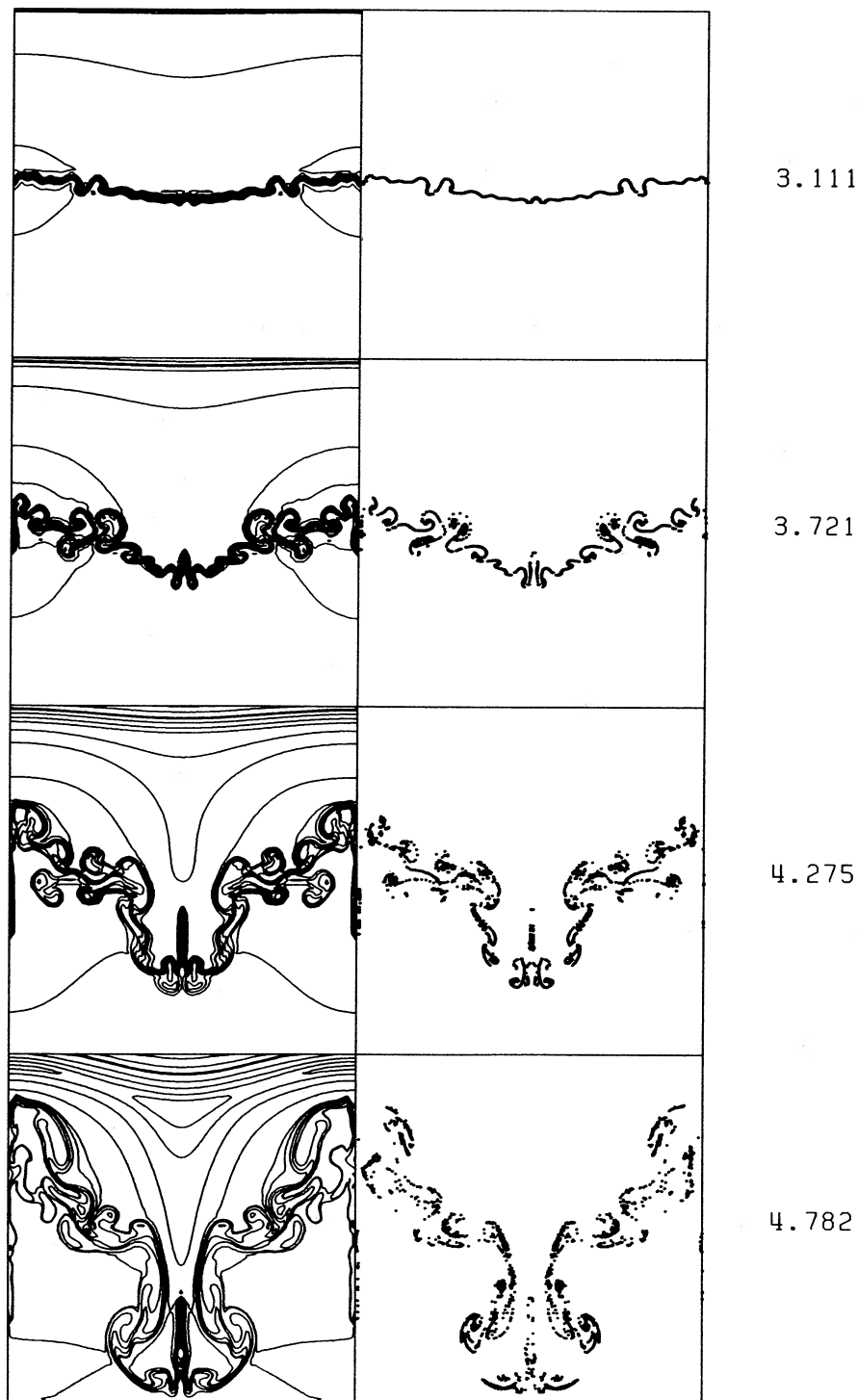


FIG. 9.—Same as Fig. 6a but for a low-resolution (128×128 grids) and a limited (lower-half) region of perturbation (run 51 in Table 1).

6.1. Dependence on the Initial Amplitude

Figure 15 depicts the mixing width against the square of time for various ϵ of random perturbation (128×128 grids). Here the density ratio is $\rho_1/\rho_2 = 3$. The mixing width, h , is defined as the distance between the upper- and lowermost marker particles which are initially placed at the interface. The mixing width is found to be very sensitive to the initial amplitude of the perturbation. This property is important for the

mixing in supernova explosions because the amplitude of the velocity perturbation is very small if convection is the source of the perturbation.

6.2. Dependence on the Perturbation Mode

Next we examine how the mixing width, h , depends on the mode of the initial perturbation. Figure 16 shows the increase in h with time for various modes (128×128 grids).

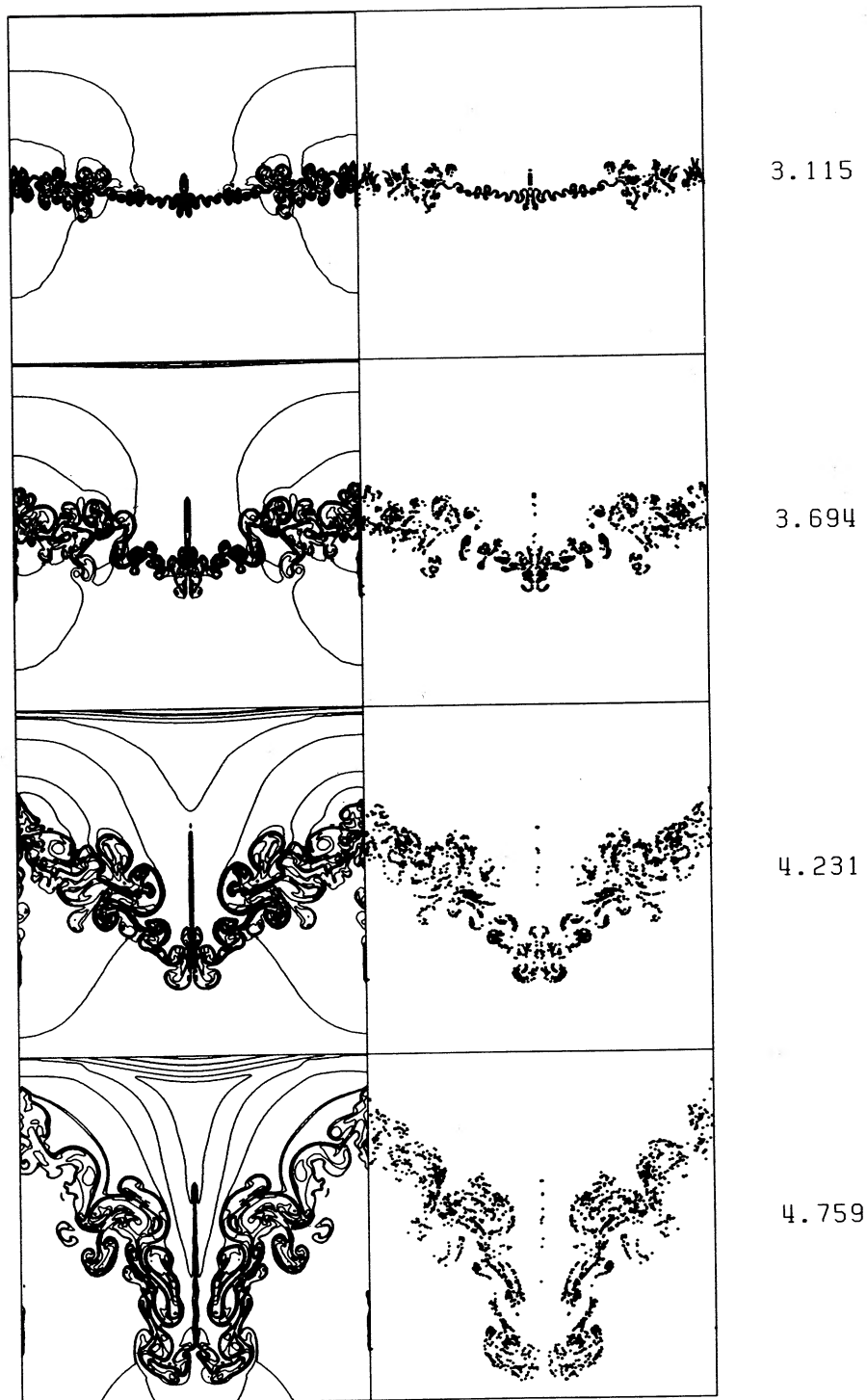


FIG. 10.—Same as Fig. 9 but for a high-resolution (256×256 grids; run 75). Fractal fingering is much more prominent than that in Fig. 9.

The low-amplitude case of $\epsilon = 10^{-3}$ is depicted in Figure 16a. The lines start at $t = 0$ tangentially to the abscissa (x -axis) and the growth of the R-T instability obeys its linear growth rate during these periods. Therefore, h grows faster in shorter waves than in longer ones for such a low amplitude, and the difference among these lines can be understood from the linear growth rate given in equation (4). The mixing width for $m = 16$ (S16) and random (R128) are almost the same until $t \sim 2$,

because the fastest growing mode in the 128×128 grids is $m \sim 16-20$ (see Fig. 5).

This difference among the modes becomes much smaller when the amplitude of the initial perturbation is increased to $\epsilon = 0.01$. In Figure 16b, we plot h for various modes. Small difference between S1 and others stems not from the linear growth rate at the very initial phase but from the nonlinear effect (the curves start with finite angles near $t = 0$). The differ-

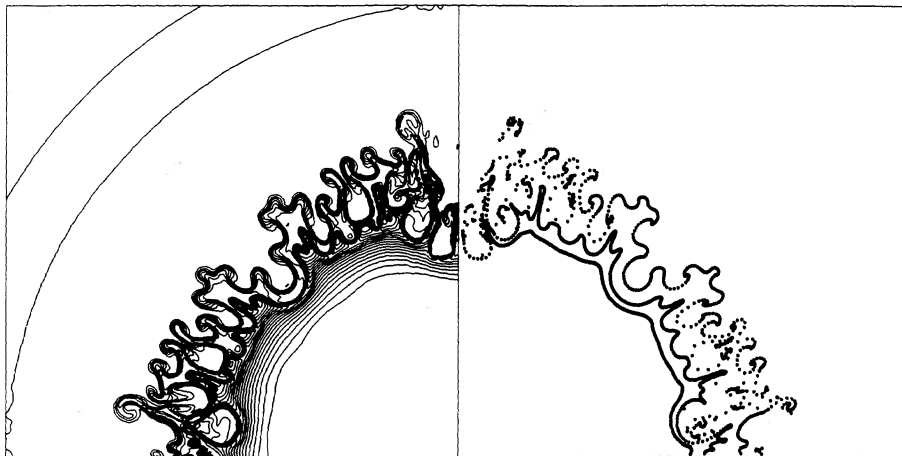


FIG. 11.—Same as Fig. 1 but for a very small initial amplitude of 0.2% and the mode of M20 ($m = 20$ of periodic). The number of grids is 1025×1025 . The time is 14,000.6 s after the explosion. The size of the box is 3.87×10^{12} cm. Note the feature of *fractal fingering* in a supernova explosion (SN1987A: model 14E1).

ence among the modes is much smaller if the initial amplitude is as large as $\epsilon = 0.16$ (see Fig. 16c), so that the mixing width is completely identical with each other at the very early stage.

We conclude that the width of the R-T mixing is almost the same among various modes if the initial amplitude exceeds 0.01. This has an important implication for the supernova problems since this suggests that the mixing width in the supernova ejecta is determined mainly by the amplitude of the initial perturbation rather than by its mode as long as each mode is finely resolved. This also suggests that even with somewhat coarse grid systems the mixing width in the supernova ejecta may be calculated sufficiently accurately as long as $\epsilon \gtrsim 0.01$. This may be the reason why the numerical experiments of the R-T mixing in SN 1987A give almost the same mixing width in spite of the differences in the initial models and in the numerical methods between the Fryxell et al. (1991) code and the Hachisu et al. (1990) code.

Note that the R-T instability leads to the formation of clumps in the supernova ejecta, which can be compared with the time scale for the escape of γ -rays and X-rays, spectral line profiles, etc., in SN 1987A. In order to obtain the accurate filling factor and clumping ratios, however, much higher resolutions than the present study are necessary.

6.3. Dependence on the Density Ratio

We plot the mixing width, h , against the square of time in Figure 17 for three different density ratios. For $\epsilon = 0.01$ (Fig. 17a), $h \approx 0.8, 0.4,$ and 0.2 at $t = 2$ for $\rho_1/\rho_2 = 10, 3,$ and 1.5 , respectively, which can be approximately scaled as

$$h \propto D = \frac{\rho_1 - \rho_2}{\rho_1 + \rho_2}. \quad (5)$$

For $\epsilon = 0.16$ (Fig. 17b), in contrast, the mixing widths deviate from this scaling law. Comparing Figures 17a and 17b, we see that the dependence of h on the density ratio is smaller for larger ϵ .

In short, the mixing develops faster for a higher density ratio though the dependence is weaker for larger initial amplitudes. For relatively small initial amplitudes ($\epsilon \lesssim 0.01$), the mixing width is approximately proportional to D as discussed in detail in the Appendix. The density ratio at the composition interface is closely related to the structure of the presupernova model

and may be a crucial factor to determine the mixing width of the R-T instability if the initial amplitudes are small.

6.4. Effects of Inverse Cascading Growth

One of the most important motivations of the present study is to examine whether or not the inverse cascading growth of the R-T instability can excite a large-scale mixing in the supernova ejecta in a short duration of deceleration. Here we try to answer this question.

If the inverse cascading growth of the R-T instability has an important effect as pointed out by Takabe (1989), the mixing width at a given time would be larger if a finer grid is used. To simulate this effect starting from the linear growth regime without being affected by numerical viscosity, we have to start our calculation from very small initial amplitudes such as $\epsilon \lesssim 10^{-3}$. Then the calculated mixing width is expected to be larger for the larger number of mesh points. Figure 18 depicts the mixing width against the square of time, t^2 , for two different mesh systems: 128×128 and 256×256 grids.

For a very small initial amplitude of $\epsilon = 10^{-6}$, there is apparently a large difference in the mixing width between the two grid systems (Fig. 18a). This is certainly a manifestation of the inverse cascading effect. However, its effect is not large in a sense that the mixing widths do not exceed those for $\epsilon = 0.01$ (Fig. 18a). For a relatively large initial amplitude of $\epsilon = 0.01$, on the other hand, the mixing width for the two grid systems are almost the same (Fig. 18a) because there is no linear growth regime for such a large initial amplitude.

We also plot the mixing width for a sinusoidal mode S1 in Figure 18b. Two grid systems (128×128 and 256×256) give almost the same result for $\epsilon = 0.01$. For $\epsilon = 10^{-3}$, the mixing width depends slightly on the grid system.

Our numerical method has a third-order accuracy when a parameter ϕ is set to be $\frac{1}{3}$ in Chakravarthy & Osher (1985). If we use $\phi = -1$ instead of $\frac{1}{3}$, the numerical scheme becomes fully upwind and second-order accurate. We have simulated the same problems of the R-T instability by changing the accuracy to second order. The results are plotted in Figure 19. The second-order accurate scheme introduces a much larger numerical viscosity than the third-order one. Two different schemes give slightly different results for $\epsilon = 10^{-6}$ but almost the same mixing width for $\epsilon = 0.01$. Note that this comparison

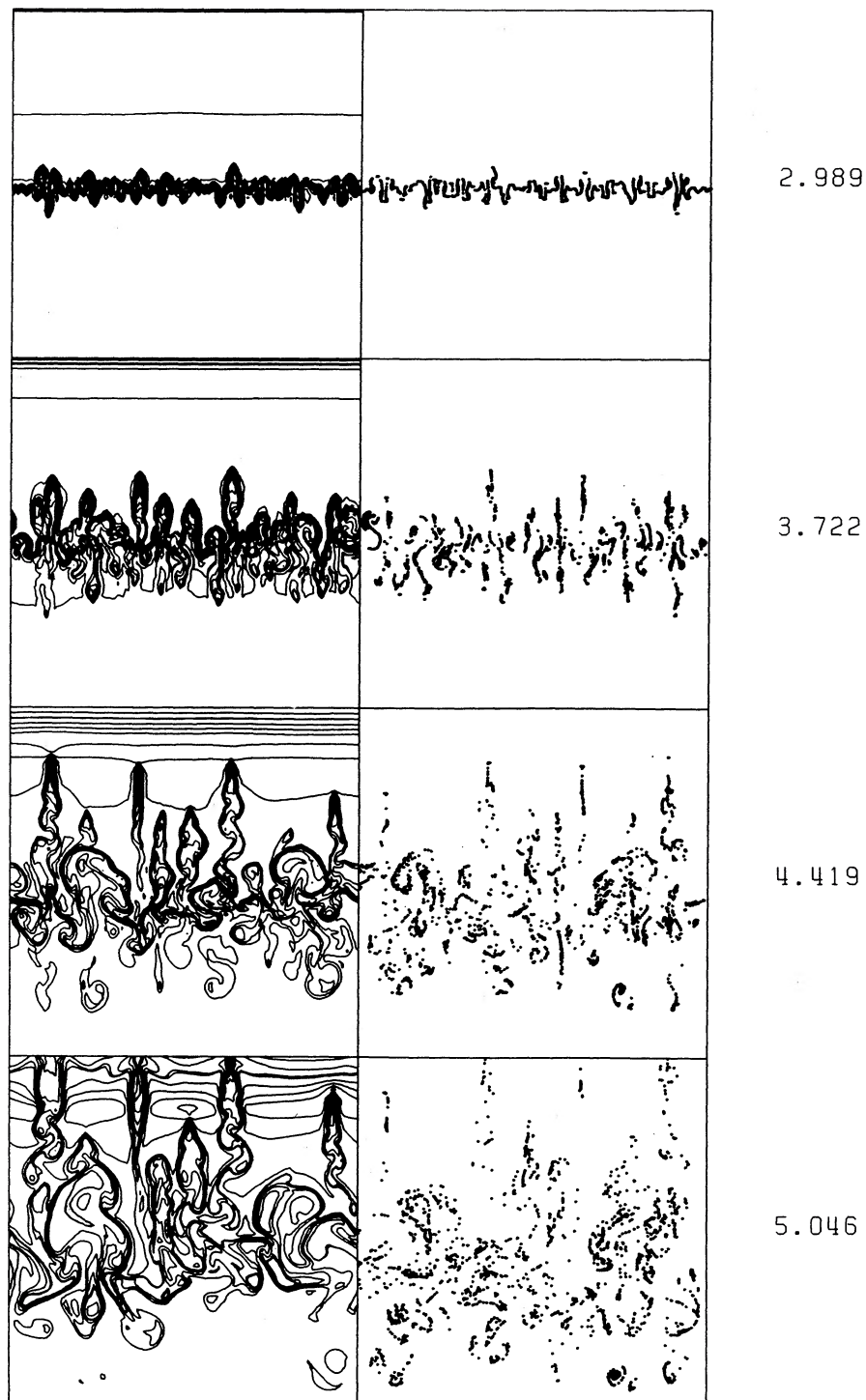
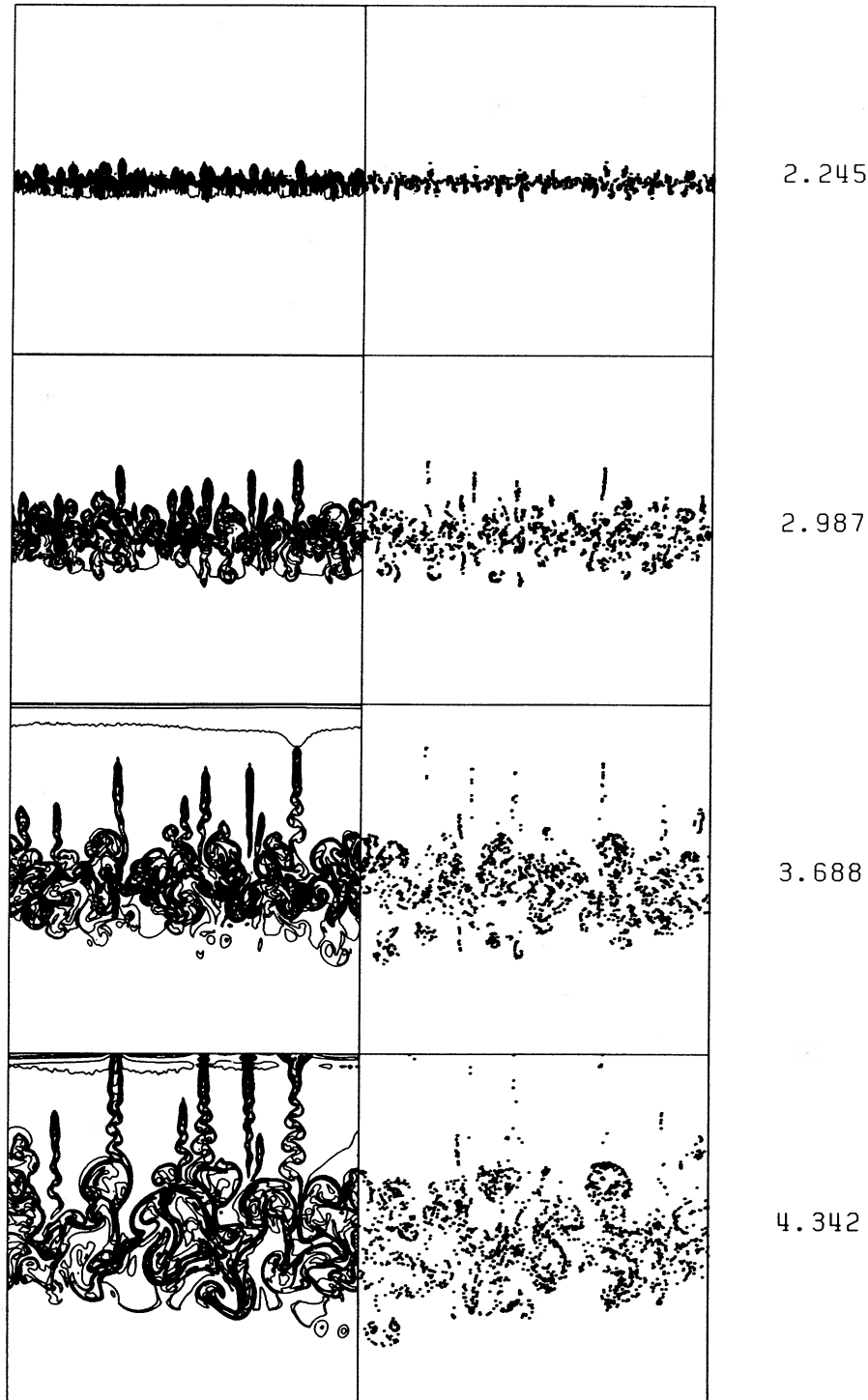


FIG. 12a

FIG. 12.—Same as Fig. 6 but for a random perturbation. (a) low-resolution (128×128 grids; run 31 in Table 1) and (b) high-resolution (256×256 grids; run 70 in Table 3). The initial amplitude is $\epsilon = 10^{-6}$ for both cases. Mixing pattern changes from small scales to large scales in time. Upward-moving streamers are made by rising small bubbles. Once this type of bubble is created and moving upward, the upward-mixing is faster than the downward-mixing.

FIG. 12*b*

is made for the same type of scheme where the flux is calculated by Roe's method. It is much more complicated to compare two results obtained by completely different numerical schemes such as the results of Fryxell et al. (1991) and Hachisu et al. (1990).

In terms of numerical viscosity, the dependence on the accuracy of numerical code is the same as that on the mesh resolution. A less accurate numerical code needs much more

grid points to produce the same quality of flow solution. Therefore, the discussion on the accuracy of the numerical code may be replaced with the discussion on the mesh resolution as done above. In this sense, the good agreement between the results of Fryxell et al. (1991) and Hachisu et al. (1990) can be naturally explained by the present results of mixing width.

Our conclusion is that the inverse cascading growth has an

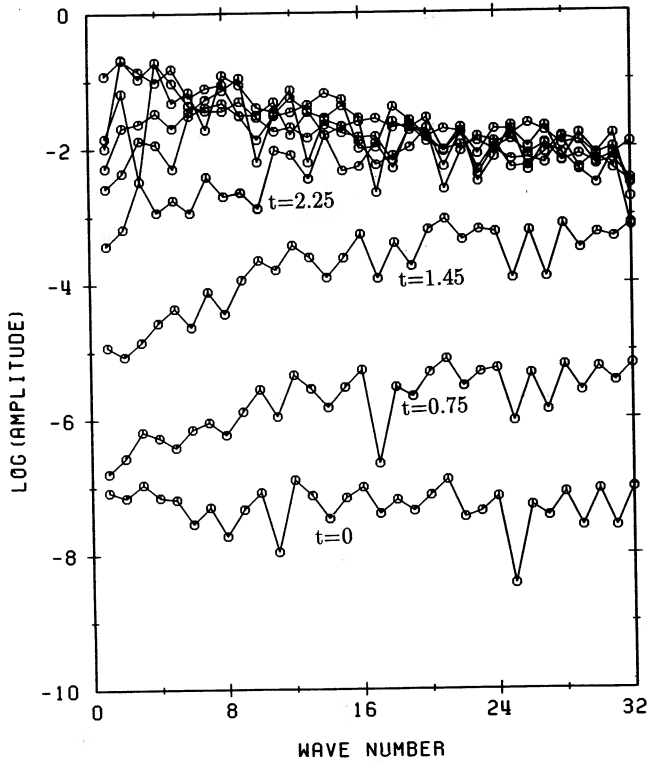


FIG. 13.—Same as Fig. 8 but for a random perturbation case of Fig. 12b (run 70 in Table 3). Shorter waves grow much faster than longer ones but saturate at $t \sim 2$.

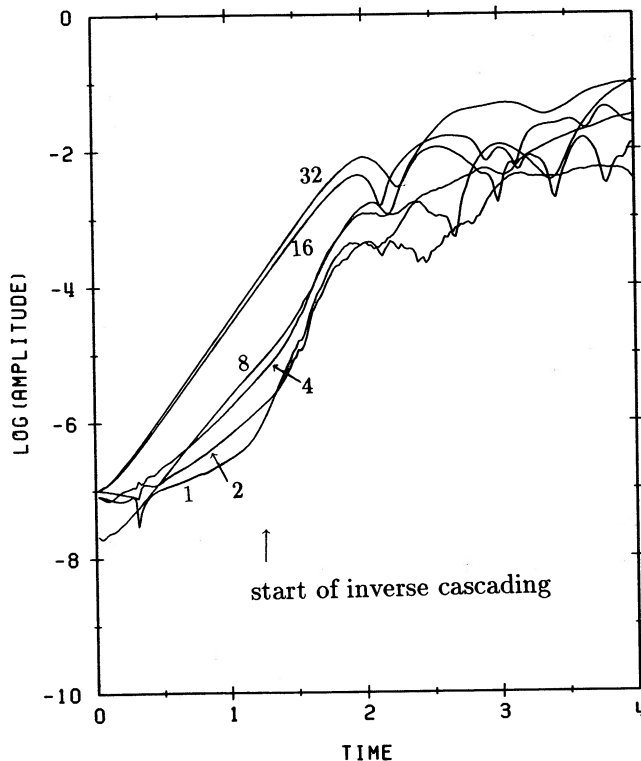


FIG. 14.—Same as Fig. 4 but for a random perturbation case of Fig. 12b (run 70 in Table 3). The growth rates for shortest waves such as $n = 16$ is well described by eq. (4) but longest waves such as $n = 1$, $n = 2$, or $n = 4$ suddenly have a larger growth rate than that described by equation (4) at $t \sim 1.5$. This is a result of nonlinear coupling.

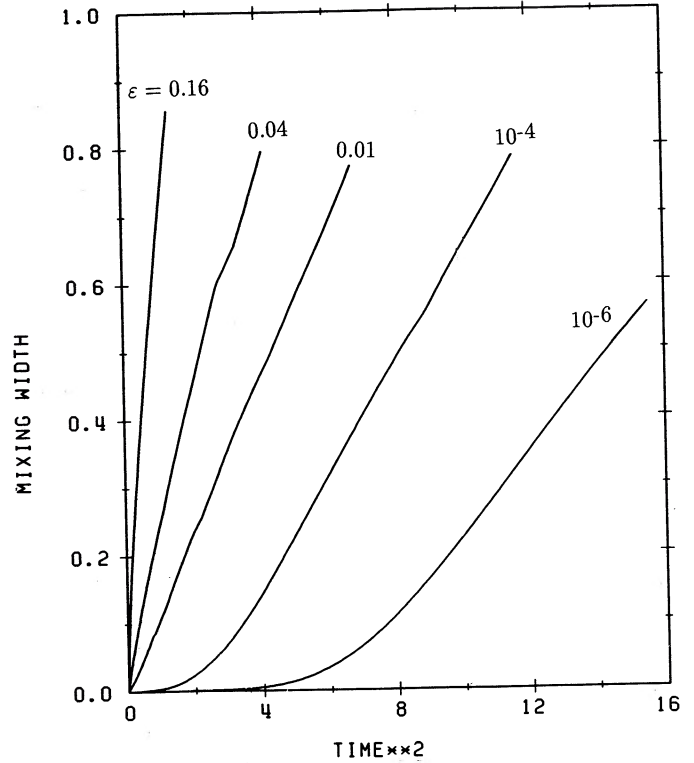


FIG. 15.—Width of the R-T mixing is plotted against the square of time for various initial amplitudes of $\epsilon = 10^{-6}$, 10^{-4} , 0.01, 0.04, and 0.16. Grid size is 128×128 . The perturbation modes are all random (runs 31–36 in Table 1). Mixing width depends strongly on the initial amplitude.

important effect if the initial amplitude is smaller than ϵ that affects the mixing width. This implies that as far as the initial amplitude as large as $\epsilon \gtrsim 0.01$ is concerned, the mixing width depends on firstly the initial amplitude and secondly the density ratio rather than the numerical accuracy. (Note that the longest waves should be finely resolved in order that the above statement is valid.) Such large initial amplitudes have been assumed to explain the R-T mixing in the ejecta of SN 1987A (e.g., Arnett et al. 1989; Hachisu et al. 1990). For these large velocity fluctuations, there is no regime of linear growth as shown in the present paper. Therefore, we conclude that we *may not* remove the difficulty mentioned in § 1 by considering the inverse cascading growth of the R-T instability.

7. CONCLUSIONS

We have numerically studied the nonlinear growth of two-dimensional Rayleigh-Taylor instabilities and applied the results to the mixing in the supernova ejecta. First, we have presented much refined calculations of mixing in the realistic model of SN 1987A by using a better code with various mesh resolutions. It is found that (1) the mixing width depends only slightly on the mesh resolution if the initial amplitude is larger than $\sim 5\%$ of the expansion speed. The results also show that (2) the mixing width due to Rayleigh-Taylor instabilities is still too small to account for the observations of SN 1987A, even with relatively large initial perturbations.

Second, we consider much simplified ideal models of R-T instabilities of compressible gas with an adiabatic constant $\gamma = 4/3$, in order to resolve the problem of too small mixing width in a realistic model of SN 1987A. The ideal R-T instabilities have been calculated for various mesh resolution, the

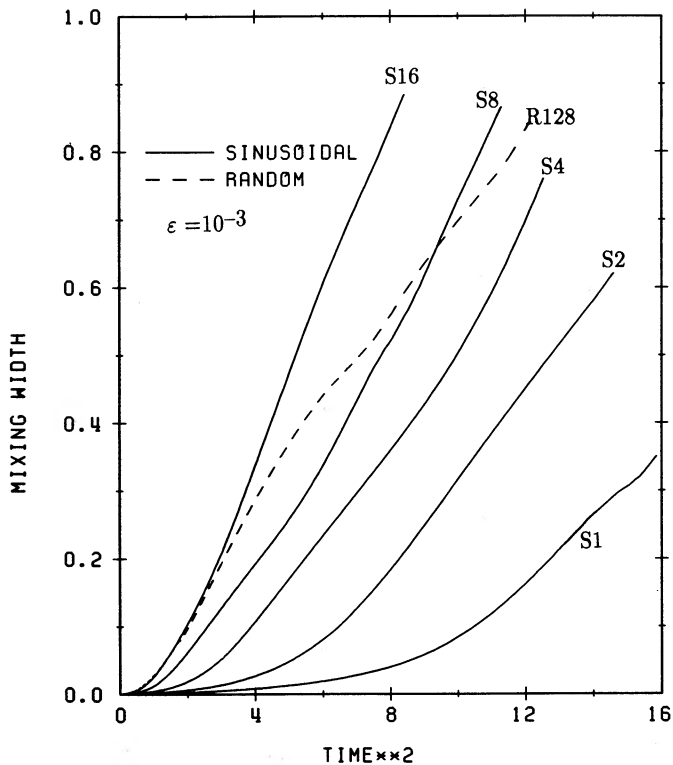


FIG. 16a

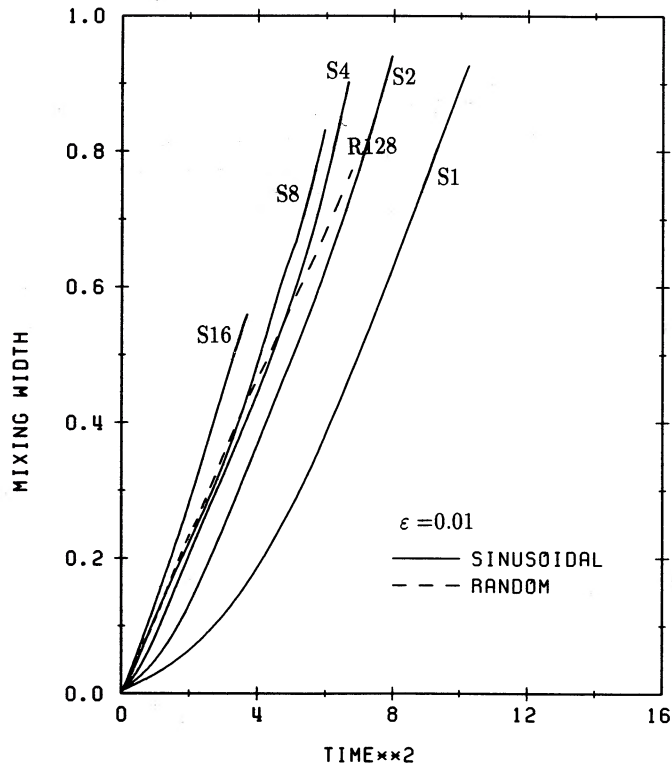


FIG. 16b

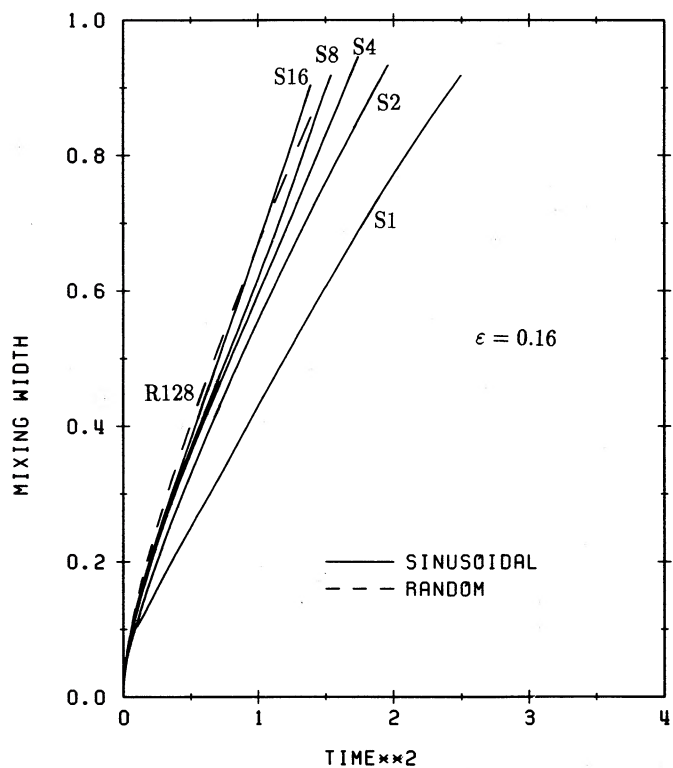


FIG. 16c

FIG. 16.—Same as Fig. 15 but for sinusoidal modes. (a) Initial amplitude of $\epsilon = 10^{-3}$ (runs 2, 7, 12, 17, 22, and 33 in Table 1); (b) $\epsilon = 0.01$ (runs 3, 8, 13, 18, 23, and 34); (c) $\epsilon = 0.16$ (runs 5, 10, 15, 20, 25, and 36). Symbols such as S1 mean the sinusoidal mode with $m = 1$. The case for a random perturbation is also added (dashed line).

numerical accuracy (second-order and third-order), the density ratio, the initial amplitude of the perturbation, and the mode of the initial perturbation (random from mesh to mesh and sinusoidal waves). The calculations have clearly demonstrated two interesting features of the Rayleigh-Taylor instability, i.e., the fractal fingering and the inverse cascading growth. The inverse cascading growth plays no important role to generate a large-scale mixing when the initial amplitude of the velocity perturbation is larger than 1% of the sound speed.

On the other hand, we have found that (1) when the initial amplitude of the velocity perturbation is larger than 1% ($\epsilon \geq 0.01$) of the sound speed, the mixing width in time depends hardly on the mesh resolution, numerical accuracy, or the mode of the initial perturbation. (2) The mixing width depends mainly on the initial amplitudes and the density ratio. This suggests that (3) the mixing width in the supernova ejecta depends mainly on the initial amplitude of the perturbation (ϵ) and on the density structure of the presupernova models (density ratio) rather than the mesh resolution. This confirms the previous results of a realistic mixing in SN 1987A.

These conclusions imply that the realistic mixing width in supernova ejecta can be calculated even with a relatively coarse grid system such as 500×500 or 1000×1000 as done by the two groups (Fryxell et al. 1991; Hachisu et al. 1990, 1991) as long as the relatively large ($\epsilon \geq 0.01$) initial amplitude is applied. (Note, however, the necessity of much higher resolutions in order to compare the calculated clumps with the related observed phenomena in SN 1987A as mentioned in § 6.2.) In the forthcoming papers, we will calculate the R-T mixing in the various types of supernova explosions and discuss the dependence of the mixing width on the structure of the supernova progenitors.

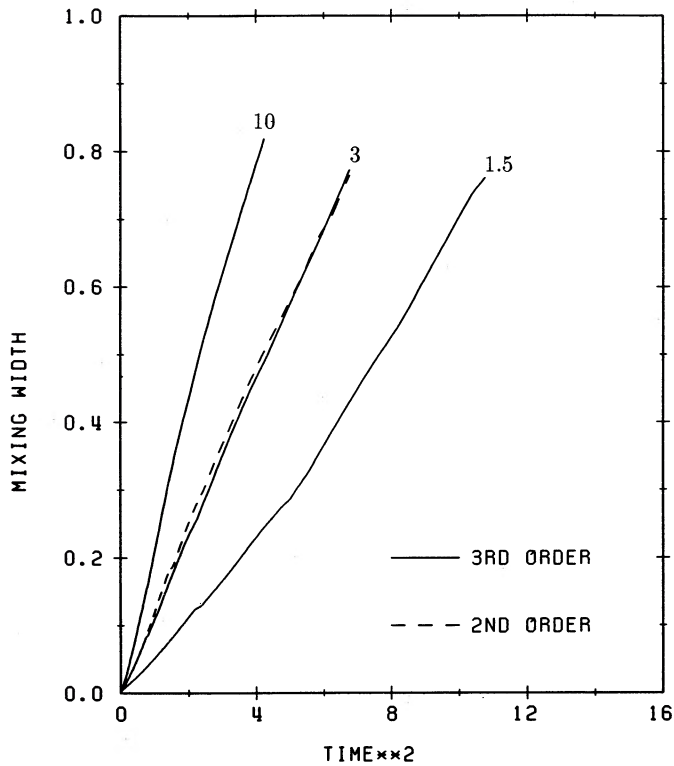


FIG. 17a

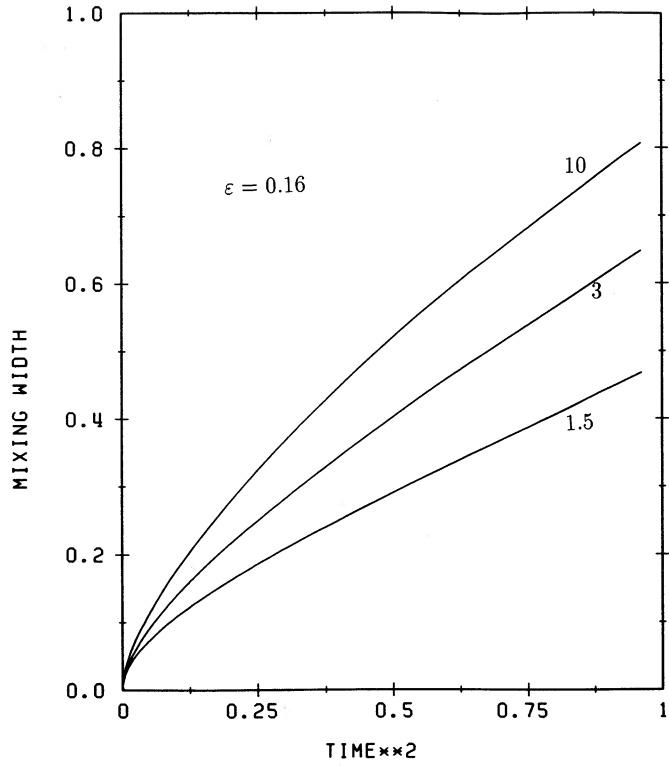


FIG. 17b

FIG. 17.—Same as Fig. 15 but for various density ratios. The attached numbers denote the density ratios of $\rho_1/\rho_2 = 10, 3,$ and 1.5 . (a) the initial amplitudes are all $\epsilon = 0.01$; (b) $\epsilon = 0.16$. A result by the second-order accuracy code is added (dashed line).

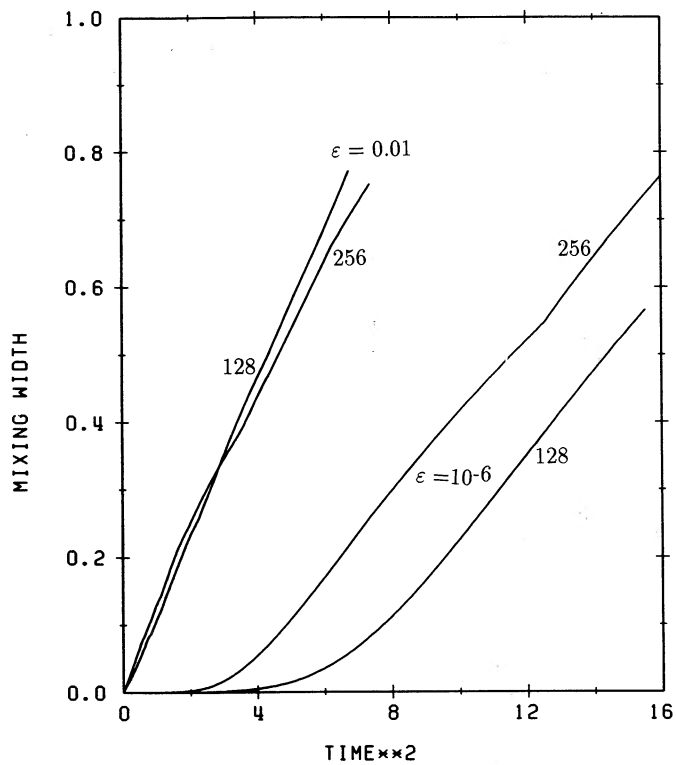


FIG. 18a

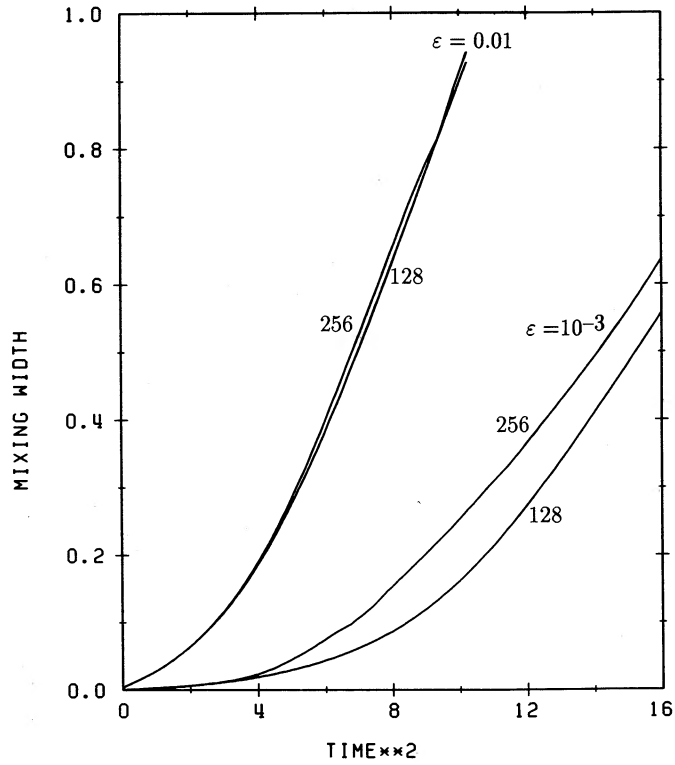


FIG. 18b

FIG. 18.—Same as Fig. 15 but for two different mesh resolutions, i.e., 128×128 and 256×256 grid systems. The numbers attached (128 and 256) denote the number of grids. (a) Random modes; (b) sinusoidal ($m = 1$) modes. If the initial amplitude is as large as 0.01, the mesh resolution has little effect on the mixing width.

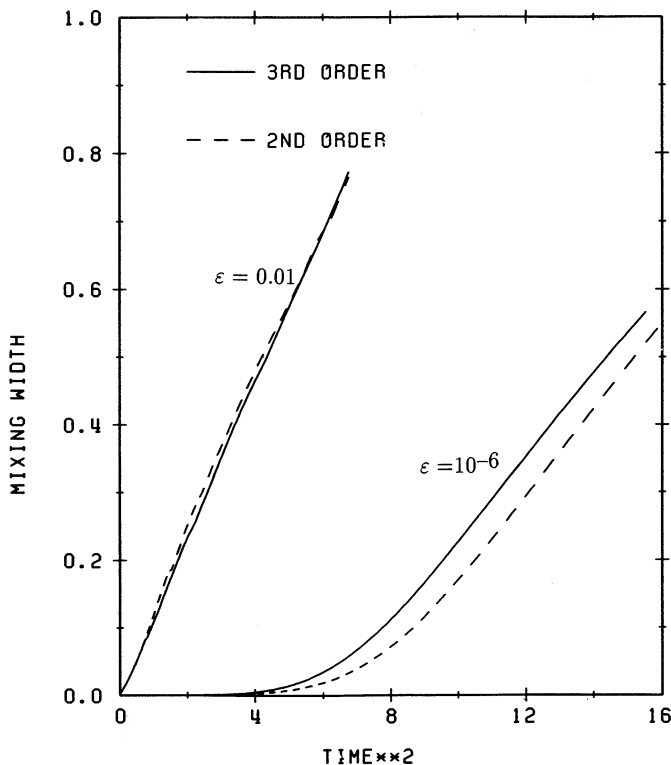


FIG. 19.—Same as Fig. 18a but for two different codes with different numerical accuracies, i.e., third-order (solid lines) and second-order (dashed lines).

We thank H. Takabe for pointing out the possibility of the inverse cascading growth of the R-T instability. The computation was carried out on a Fujitsu VP-400E vector processor of the Data Processing Center of Kyoto University, on a VP-200 vector processor of the Institute of Space and Astronautical Sciences (ISAS), and on a VP-400E of the Kansai Institute of

Computational Fluid Dynamics (KiCFD). This work has been supported in part by the Grant-in-Aid for Scientific Research (02234206, 02302024, 02640204, 03218202, 03218205) of the Japanese Ministry of Education, Science, and Culture, by the Space Data Analysis Center of ISAS, and also by the KiCFD.

APPENDIX

A SCALING LAW OF MIXING WIDTH

Upward- and downward-mixings are symmetric to the original surface at the initial stages of mixing as seen in Figures 12a and 12b. In the later phases, however, the upward-mixing becomes faster than the downward as seen in Figures 20a and 20b. The width of mixing is plotted against the square of time, gt^2 , in Figure 20a and against Dgt^2 in Figure 20b. We note that the upward-mixing (solid line) grows linearly at the later phase of mixing, while the downward-mixing slows down after its width reaches 10% of the box size.

TABLE 4
COEFFICIENT OF MIXING WIDTH (RANDOM)

Number of Run	Mesh	ρ_1/ρ_2	ϵ	β
31.....	128	3	10^{-6}	0.070
32.....	128	3	10^{-4}	0.11
34.....	128	3	0.01	0.15
35.....	128	3	0.04	0.23
36.....	128	3	0.16	0.57
70.....	256	3	10^{-6}	0.077
71.....	256	3	10^{-3}	0.079
72.....	256	3	0.01	0.13
73.....	256	10	10^{-6}	0.082
74.....	256	1.5	10^{-6}	0.081

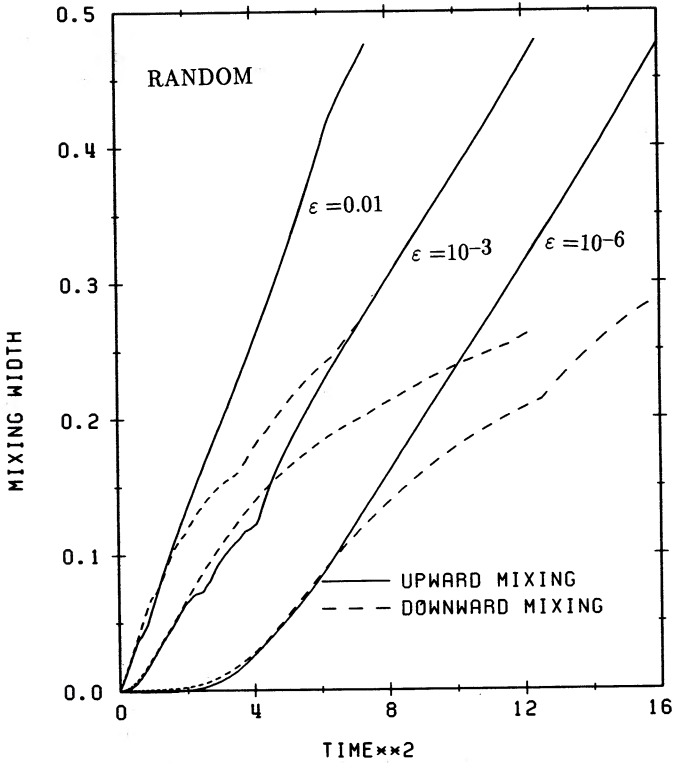


FIG. 20a

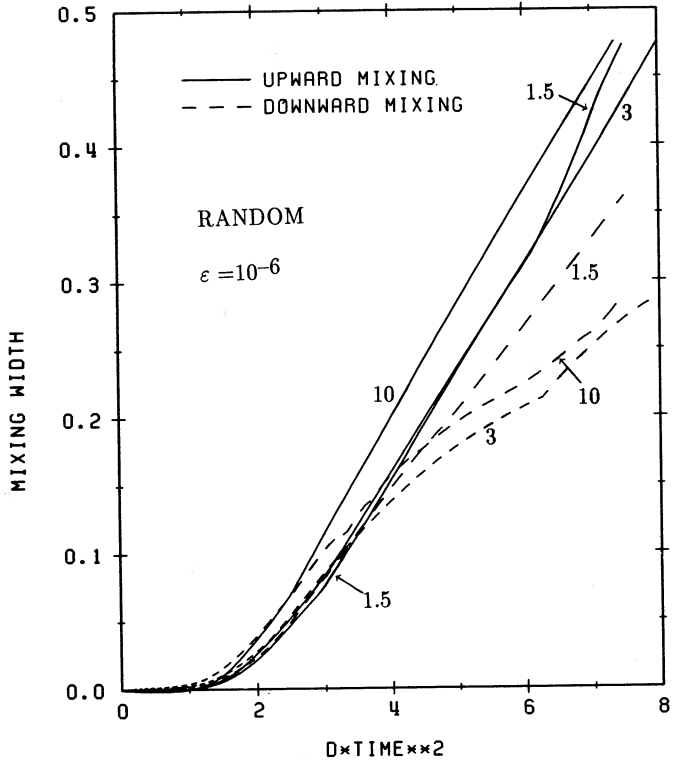


FIG. 20b

FIG. 20.—Upward-mixing (solid lines), h_1 , and downward-mixing (dashed lines), h_2 , are plotted against the square of time (a), gt^2 , or against the scaled square of time (b), Dgt^2 . The perturbation modes are all random. Grid size is 256×256 . The upward-mixings linearly grow in the later phase. The density ratio is $\rho_1/\rho_2 = 3$ for all models in Fig. 20a. There exists a scaling law on the upward-mixing for small initial amplitudes as seen in Fig. 20b. The numbers attached in Fig. 20b denote the density ratios.

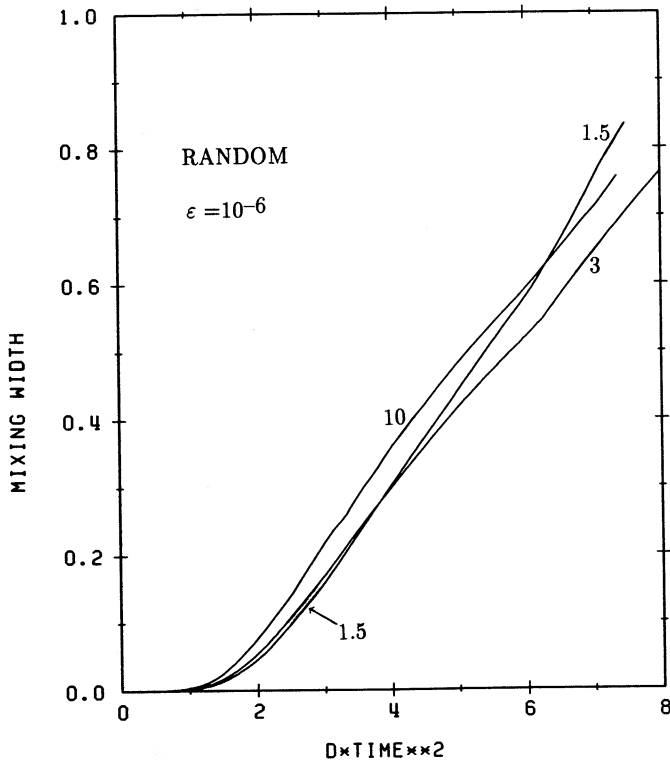


FIG. 21.—Total (upward plus downward) width of mixing is plotted as a function of the scaled square of time, i.e., Dgt^2 . There also exists a scaling law on the total width of mixing. Grid size is 256×256 . The numbers attached denote the density ratios.

The experiments of the R-T instability has already suggested that the width of the upward-mixing is proportional to the square of time (e.g., Read 1984; Youngs 1984) as

$$h_1 = \beta(X - X_0), \quad (6)$$

where

$$X = Dgt^2. \quad (7)$$

Here h_1 is the width of upward-mixing from the original level. The coefficient β is 0.07 while it varies little with the density ratio.

Figures 20a and 20b clearly show the linearity of the upward-mixing in the later phase confirming the above experimental statement. Thus the values of β can be estimated from these figures as listed in Table 4. For 256×256 grids, $\beta \sim 0.08$ when the initial amplitude, ϵ , is smaller than 10^{-3} . This value of β is almost independent of the density ratio and ϵ if ϵ is very small. If $\epsilon \gtrsim 10^{-3}$, however, β becomes larger than 0.07. For example, β is ~ 0.13 for $\epsilon = 0.01$.

Defining the mixing width by the sum of the upward- and downward-mixing, i.e., $h = h_1 + h_2$, we plot the mixing width against Dgt^2 in Figure 21. As expected from Figure 20a, three mixing widths almost coincide with one another for a very small initial amplitude of $\epsilon = 10^{-6}$ (Fig. 21). This clearly confirms the existence of a scaling law for total mixing. The scaling law breaks down for such a large initial amplitude as $\epsilon \gtrsim 0.16$ (see Fig. 17b). Then the differences in these three widths of mixing become small as the initial amplitude increases.

REFERENCES

- Arnett, W. D., Fryxell, B. A., & Müller, E. 1989, *ApJ*, 341, L63
 Chandrasekhar, S. R., & Osher, S. 1985, AIAA Paper, No. 85-0363
 Chandrasekhar, S. 1961, *Hydrodynamic and Hydromagnetic Stability* (Oxford: Oxford Univ. Press), Chap. X-XI
 Den, M., Yoshida, T., & Yamada, Y. 1990, *Prog. Theor. Phys.*, 83, 723
 Filippenko, A. V., & Sargent, W. L. W. 1989, *ApJ*, 345, L43
 Fryxell, B. A., Müller, E., & Arnett, W. D. 1991, *ApJ*, 367, 619
 Hachisu, I., Matsuda, T., Nomoto, K., & Shigeyama, T. 1990, *ApJ*, 358, L57
 ———. 1991, *ApJ*, 368, L27
 Herant, M., & Benz, W. 1991, *ApJ*, 370, L81
 ———. 1992, *ApJ*, in press
 Kumagai, S., Shigeyama, T., Nomoto, K., Itoh, M., Nishimura, J., & Tsuruta, S. 1989, *ApJ*, 345, 412
 Mitchner, M., & Landshoff, R. K. M. 1964, *Phys. Fluids*, 7, 862
 Müller, E., Fryxell, B., & Arnett, W. D. 1992, *A&A*, in press
 Plesset, M. S., & Hsieh, D.-Y. 1964, *Phys. Fluids*, 7, 1099
 Read, K. I. 1984, *Physica*, 12D, 45
 Sharp, D. H. 1984, *Physica*, 12D, 3
 Shigeyama, T., & Nomoto, K. 1990, *ApJ*, 360, 242
 Shigeyama, T., Nomoto, K., Tsujimoto, T., & Hashimoto, M. 1990, *ApJ*, 361, L23
 Takabe, H. 1989, private communication
 Tueller, J., Barthelmy, S., Gehrels, N., Teegarden, B. J., Leventhal, M., & MacCallum, C. J. 1990, *ApJ*, 351, L41
 Wang, Y.-M., & Robertson, J. A. 1985, *ApJ*, 299, 85
 Witterborn, F. C., Bregman, J. D., Wooden, D. H., Pinto, P. A., Rank, D. M., Woosley, S. E., & Cohen, M. 1989, *ApJ*, 338, L9
 Yamada, Y., Nakamura, T., & Oohara, K. 1990, *Prog. Theor. Phys.*, 84, 436
 Youngs, D. L. 1984, *Physica*, 12D, 32